



# Innovative and Sustainable Groundwater Management in the Mediterranean

## D3.2 Report on Surrogate Models in the Case Studies

VERSION 2



**Acknowledgment:** This project is part of the PRIMA Programme supported by the European Union's Horizon 2020 Research and Innovation Programme under Grant Agreement No 1923.

**Disclaimer:** The content of this publication is solely responsibility of the authors and it does not represent the view of the PRIMA Foundation.

**DOI:** 10.5281/zenodo.7674923

## Project Information

Project Title	Innovative and Sustainable Groundwater Management in the Mediterranean		
Project Acronym	InTheMED	Grant Agreement Number	1923
Program	Horizon 2020		
Type of Action	Water RIA – Research and Innovation Action		
Start Date	March 1, 2020	Duration	36 months
Project Coordinator	Universitat Politècnica de València (UPV), Spain		
Consortium	<p>Universitat Politècnica de València (UPV), Spain</p> <p>Helmholtz-Zentrum für Umweltforschung (UFZ), Germany</p> <p>Università degli Studi di Parma (UNIPR), Italy</p> <p>Boğaziçi Üniversitesi (BU), Turkey</p> <p>Centre de Recherches et des Technologies des Eaux (CERTE), Tunisie</p> <p>Technical University of Crete (TUC), Greece</p> <p>Associação do Instituto Superior Técnico para a Investigação e Desenvolvimento (IST-ID), Portugal</p>		

## Document Information

Deliverable Number	D3.2	Deliverable Name	Report on Surrogate Models in the Case Studies	
Work Package number	WP3	Work Package Title	Innovative Smart Modelling in the MED	
Due Date	Contractual (revised)	May, 2022	Actual	February, 2023
Version Number	2.0			
Deliverable Type	Report (R)	Dissemination Level	Public (PU)	
Authors	Valeria Todaro Daniele Secci Marco D’Oria Maria Giovanna Tanda Andrea Zanini			
Co-Authors	Janire Uribe Asarta, J. Jaime Gómez-Hernández, Vanessa Almeida Godoy (UPV) Onur Cem Yologlu, Nadim K Coptý, Irem Daloglu Cetinkaya, Ali Kerem Saysel (BU) Emmanouil A. Varouchakis, George P Karatzas, Paraskevas Diakoparskevas, Ioanna Anyfanti (TUC) Leonardo Azevedo, Lino Pereira João (IST-ID)			
Reviewer(s)	All			

## Document History

Version	Date	Stage	Reviewed by
1.0	2022/05/31	First version	All
2.0	2023/02/24	Second version	All

## Table of Contents

Project Information.....	2
Document Information .....	3
Document History .....	3
List of Tables.....	5
List of Figures.....	6
Executive Summary.....	10
1. Introduction .....	11
2. Case Studies .....	12
2.1. Requena-Utiel .....	12
2.2. Tympaki (Greece).....	19
2.3. Konya (Turkey) .....	32
2.4. Grombalia (Tunisia).....	44
2.5. Castro Verde (Portugal).....	57
3. References .....	79



## List of Tables

Table 1. Mean cross-validation scores for each fold.....	17
Table 2. Average STRK prediction statistical measures for using the product–sum space–time variogram in terms of ME, mean error; MAE, mean absolute error; MARE, mean absolute relative error; RMSE, root mean square error; $R^2$ , coefficient of determination.....	26
Table 3. Tunisia: station name and station code of the gauging stations.....	46
Table 4. Tunisia: name and codes of the monitoring wells .....	48
Table 5. Tunisia: datasets of quality data. ....	49
Table 6. Tunisia: exploitation rate data. ....	50
Table 7. Portugal: name, code, and reference of the meteorological stations, as well as frequency of measurements, for an overall period between 1970-2021 (SNIRH).....	58
Table 8. Portugal: Name, code, and reference of the piezometric stations, as well as frequency of measurements taken for an overall period between 1997-2022(SNIRH) .....	63

## List of Figures

Figure 1. Requena-Utiel aquifer and its lateral limits.....	13
Figure 2. Part of the generated dataset used for training the surrogate model.....	15
Figure 3a. Mean regression score obtained by using Random Forest (RF), AdaBoost (AB), and XGBoost (XB); 3b. Mean square error over 64 scenarios. ....	17
Figure 4. Mean CPU time required to calculate and get the piezometric head values.....	18
Figure 5. Piezometric heads obtained with MODFLOW (test data) and with the surrogate model (Random Forest) .....	18
Figure 6. All the wells along with the representative ones for each group .....	19
Figure 7. Pumping wells spatial distribution.....	20
Figure 8. Observation wells with calibration – validation data available .....	21
Figure 9. Salt water intrusion zone 2009 .....	22
Figure 10. Simulation results wet period October 2019- March 2020 .....	22
Figure 11. Simulation results dry period April 2020-September 2020.....	23
Figure 12. Simulated hydraulic heads at the observation wells .....	23
Figure 13. Space–time variogram fit (stars) using the product–sum model .....	25
Figure 14. Groundwater level spatial distribution, meters above sea level, for the wet period of October 2019-March 2020.....	26
Figure 15. Groundwater level spatial distribution, meters above sea level, for the dry period of April 2020-September 2020.....	27
Figure 16. Spatial distributions of observations and their related cluster.....	30
Figure 17. Root Mean Squared Error for Different Clusters/Topologies .....	30
Figure 18. Variograms for cluster 1-2,3-4,5-6 .....	31
Figure 19. Spatial variability of hydraulic head (meters above sea level) in the area of Tympaki using SOM-OK approach.....	32
Figure 20. Location Map and Surface Elevation of Konya Closed Basin.....	33
Figure 21. Average Annual Precipitation of Konya Closed Basin (1970-2020) .....	33
Figure 22. Satellite land use map of Konya Closed Basin for year of 2018.....	34
Figure 23. Monthly Precipitation Distribution over the Konya Closed Basin for selected year/months. Dots show location of available meteorological stations.....	36
Figure 24. Hydraulic Conductivity of Konya Closed Basin.....	37
Figure 25. Comparison of the simulated and observed heads.....	38
Figure 26. Spatial distribution of the simulated head on January of years 2000, 2005, 2010, 2015 and 2020 .....	39
Figure 27. Control Points for Surrogate Model .....	40
Figure 28. Training, validation and test performances of the ANN for the period 2000-2019 .....	41
Figure 29. Groundwater level variations vs time at control point 2 for different precipitation scenarios: observed (Prec) and -/+ 20%. The solid black line depicts the variation of groundwater levels considering the observed (2000-2009) water demand. The grey band	

shows the variability of the predicted groundwater levels inside the range +/- 20% of the water demand .....	41
Figure 30. Groundwater level variations vs time at control point 10 for different precipitation scenarios: observed (Prec) and +/- 20%. The solid black line depicts the variation of groundwater levels considering the observed (2000-2009) water demand. The grey band shows the variability of the predicted groundwater levels inside the range +/- 20% of the water demand .....	42
Figure 31. Groundwater level variations vs time at control point 20 for different precipitation scenarios: observed (Prec) and +/- 20%. The solid black line depicts the variation of groundwater levels considering the observed (2000-2009) water demand. The grey band shows the variability of the predicted groundwater levels inside the range +/- 20% of the water demand .....	42
Figure 32. Groundwater level variations vs time at control point 30 for different precipitation scenarios: observed (Prec) and +/- 20%. The solid black line depicts the variation of groundwater levels considering the observed (2000-2009) water demand. The grey band shows the variability of the predicted groundwater levels inside the range +/- 20% of the water demand .....	43
Figure 33. Training, validation and test performances of the ANN for the period 2020-2039	44
Figure 34. Tunisia: study area and location of the temperature and rain stations and monitoring wells.....	46
Figure 35. Tunisia: SPEIs for time windows of 3, 6, 9, 12, 18, 24 and 36 months .....	47
Figure 36. Tunisia: Groundwater levels (m a.s.l.) recorded in the period 2000-2020. The points are the observations and the solid line is the regression line .....	49
Figure 37. Tunisia: Nitrate recorded in the period 2009-2019. The points are the observations and the solid line is the regression line.....	50
Figure 38. Tunisia: Pearson correlation coefficients between groundwater levels observed at the 23 wells (y-axis) and the and SPEIs at the time scale of 3, 6, 9, 12, 18, 24 and 36 months (x-axes) considering all months (a) and February-April months, respectively.....	52
Figure 39. Tunisia: linear regression model for the well 12440. The x-axis shows the SPEI values and the y-axis the groundwater level in m a.s.l. The points are the observed groundwater levels, the solid line is the regression line and the dashed lines are the confidence intervals (95%); the correlation coefficients are reported in the boxes.....	53
Figure 40. Tunisia: linear regression model for the well 2183. The x-axis shows the SPEI values and the y-axis the groundwater level in m a.s.l. The points are the observed groundwater levels, the solid line is the regression line and the dashed lines are the confidence intervals (95%); the correlation coefficients are reported in the boxes .....	53
Figure 41. Tunisia: linear regression model for the well 2171. The x-axis shows the SPEI values and the y-axis the groundwater level in m a.s.l. The points are the observed groundwater levels, the solid line is the regression line and the dashed lines are the confidence intervals (95%); the correlation coefficients are reported in the boxes .....	54

Figure 42. Tunisia: linear regression model for the well 2543. The x-axis shows the SPEI values and the y-axis the groundwater level in m a.s.l. The points are the observed groundwater levels, the solid line is the regression line and the dashed lines are the confidence intervals (95%); the correlation coefficients are reported in the boxes .....	54
Figure 43. Tunisia: linear regression model for the well 2008. The x-axis shows the SPEI values and the y-axis the groundwater level in m a.s.l. The points are the observed groundwater levels, the solid line is the regression line and the dashed lines are the confidence intervals (95%); the correlation coefficients are reported in the boxes .....	55
Figure 44. Tunisia: linear regression model for the well 8844. The x-axis shows the SPEI values and the y-axis the groundwater level in m a.s.l. The points are the observed groundwater levels, the solid line is the regression line and the dashed lines are the confidence intervals (95%); the correlation coefficients are reported in the boxes .....	55
Figure 45. Tunisia: linear regression model for the well 2379. The x-axis shows the SPEI values and the y-axis the groundwater level in m a.s.l. The points are the observed groundwater levels, the solid line is the regression line and the dashed lines are the confidence intervals (95%); the correlation coefficients are reported in the boxes .....	56
Figure 46. Tunisia: linear regression model for the well 12405. The x-axis shows the SPEI values and the y-axis the groundwater level in m a.s.l. The points are the observed groundwater levels, the solid line is the regression line and the dashed lines are the confidence intervals (95%); the correlation coefficients are reported in the boxes.....	56
Figure 47. Portugal: study area and location of the selected temperature and rain stations and monitoring wells. ....	57
Figure 48. Portugal: study area and locations of the meteorological and piezometric stations (SNIRH).....	58
Figure 49. Portugal: groundwater levels (m a.s.l.) recorded in the period 1997-2021. The points are the observations and the solid line is the regression line.....	72
Figure 50. Portugal: SPEIs for time windows of 1, 3, 6, 9, 12, 18, 24 and 36 months.....	73
Figure 51. Portugal: Pearson correlation coefficients between groundwater levels observed at the 23 wells (y-axis) and the and SPEIs at the time scale of 1, 3, 6, 9, 12, 18, 24 and 36 months (x-axes) considering all months (left) and February-April months (right).....	75
Figure 52. Portugal: linear regression model for the well 581/41. The x-axis shows the SPEI values and the y-axis the groundwater level in m a.s.l. The points are the observed groundwater levels, the solid line is the regression line and the dashed lines are the confidence intervals (95%); the correlation coefficients are reported in the boxes.....	76
Figure 53. Portugal: linear regression model for the well 400/7. The x-axis shows the SPEI values and the y-axis the groundwater level in m a.s.l. The points are the observed groundwater levels, the solid line is the regression line and the dashed lines are the confidence intervals (95%); the correlation coefficients are reported in the boxes.....	76
Figure 54. Portugal: linear regression model for the well 512/32. The x-axis shows the SPEI values and the y-axis the groundwater level in m a.s.l. The points are the observed	

groundwater levels, the solid line is the regression line and the dashed lines are the confidence intervals (95%); the correlation coefficients are reported in the boxes.....	77
Figure 55. Portugal: linear regression model for the well 513/34. The x-axis shows the SPEI values and the y-axis the groundwater level in m a.s.l. The points are the observed groundwater levels, the solid line is the regression line and the dashed lines are the confidence intervals (95%); the correlation coefficients are reported in the boxes.....	77
Figure 56. Portugal: linear regression model for the well 524/49. The x-axis shows the SPEI values and the y-axis the groundwater level in m a.s.l. The points are the observed groundwater levels, the solid line is the regression line and the dashed lines are the confidence intervals (95%); the correlation coefficients are reported in the boxes.....	78
Figure 57. Portugal: linear regression model for the well 600/24. The x-axis shows the SPEI values and the y-axis the groundwater level in m a.s.l. The points are the observed groundwater levels, the solid line is the regression line and the dashed lines are the confidence intervals (95%); the correlation coefficients are reported in the boxes.....	78

## Executive Summary

The overall objective of the InTheMED project is to implement innovative and sustainable management tools and remediation strategies for MED aquifers (inland and coastal) in order to mitigate anthropogenic and climate-change threats by creating new long-lasting spaces of social learning among different interdependent stakeholders, NGOs, and scientific researchers in five field case studies. These are located at the two shores of the MED basin, namely in Spain, Greece, Portugal, Tunisia, and Turkey.

InTheMED will develop an inclusive process that will establish an ensemble of innovative assessment and management tools and methodologies including a high-resolution monitoring approach, smart modelling, a socio-economic assessment, web-based decision support systems (DSS) and new configurations for governance to validate efficient and sustainable integrated groundwater management in the MED considering both the quantitative and qualitative aspects.

This deliverable, namely D3.2, summarizes the activities carried out in Task 3.2: “Training and Validation of the Models in the Case Studies” (Lead: UNIPR/ participants: UPV, UFZ, TUC, IST-ID, CERTE and BU). The aim of D3.2 is to outline the surrogate models implemented for each study case. Their evaluation and performance are discussed. Two types of smart models were developed: the first type is developed based on long-time historical data, the so-called data-driven models; the second one is built on the basis of available numerical model. For each pilot site, the objectives of the surrogate model, the description of the complete numerical model or available data, the description of the surrogate model and the evaluation of the performance are presented.

## 1. Introduction

InTheMED focuses on the development of new simplified smart models that allow analysing alternative scenarios and making decisions under uncertain future conditions with small computational effort. Numerical models are crucial for the description of groundwater processes and the configuration of management scenarios. However, they need the knowledge of several factors that are often difficult to quantify and they require a large computation time to be run. The surrogate models aim to replace the numerical models allowing to perform several quick evaluations of the groundwater condition under different scenarios. These new models are built on the basis of long-time historical data and/or detailed numerical models with the aim to provide specific answers tailored to the stakeholder needs.

For each case study, a specific surrogate model addressing the particular problem of the site is built. For Requena-Utiel (Spain), Konya (Turkey) and Tympaki (Greece), surrogate models based on the results of complete numerical models have been developed. The first and second case study use machine learning algorithms, in particular, Random Forest and Artificial Neural Network. The third one is a spatiotemporal geostatistical model. For Grombalia (Tunisia) and Castro Verde (Portugal), the numerical models are not available and data-driven surrogate models were developed using a statistical approach that aims to use regression models to assess the impact of the climate change on the groundwater level.

The smart and calibrated models will be used in Task 3.4 to analyse the effects of climate change and hypothetical scenarios of socio-economic activities that may induce a change in groundwater resources. Impacts of the anthropogenic actions cannot be considered in the surrogate models developed for Grombalia (Tunisia) and Castro Verde (Portugal).

## 2. Case Studies

### 2.1. Requena-Utiel

#### Objectives of the Surrogate Model

---

In the Requena-Utiel aquifer, Spain, there is a problem with the continuous decline of piezometric heads in the aquifer, which may worsen due to the effects of climate change. In that situation, numerical models are fundamental for the determination of best management scenarios; however, their configuration, build and run require large computational time in addition to specialized knowledge. The surrogate model implemented here will replace the numerical models with a quick, easy-to-use, reliable tool. Such a tool will be used to analyse the impact of future climate scenarios and groundwater use in the piezometric heads.

#### Description of the Complete Numerical Model

---

The model domain consists of two groundwater aquifers, Requena-Utiel and Cabrillas-Malacara, which are delimited by the Water Framework Directive and the Júcar Basin authority as basic management units. Here the two aquifers were considered together due to the relevance of their hydraulic connection and from here on we refer to both just as Requena-Utiel aquifer.

The model domain is discretized into a regular mesh of square cells of 500 x 500 m<sup>2</sup> made up of 127 columns, 99 rows and 3 layers that rest on an impermeable bed of Keuper facies. The upper aquifer is quaternary, free and composed of detrital materials from the alluvial of the Magro River and glacia from the Utiel mountains. The lower aquifer is a Miocene aquifer divided into two systems. The upper system is a calcareous Miocene aquifer, free and composed of Pontian limestone and the lower system is a base conglomerate Miocene aquifer. It behaves as a confined or semi-confined aquifer, depending on the site. It is composed of alternating levels of conglomerates and sandstones with clayey sections and conglomerates of the tertiary formation.

The lateral limits correspond to the interactions between the aquifers under study and the adjacent ones. In the north, there is the Mira aquifer, and there is an estimated flux towards the Requena-Utiel aquifer of 11 hm<sup>3</sup>/year. In the southeast, there is an estimated flux from



Requena-Utiel to Buñol-Cheste of  $24 \text{ hm}^3/\text{year}$ . Based on piezometers located around the studied aquifer and on the estimated flux, the conductance values were calibrated, and the head-dependent flux boundaries were defined to be used in the north and southeast boundaries. The rest of the limits are considered impermeable. Figure 1 shows the studied aquifer and its lateral limits.

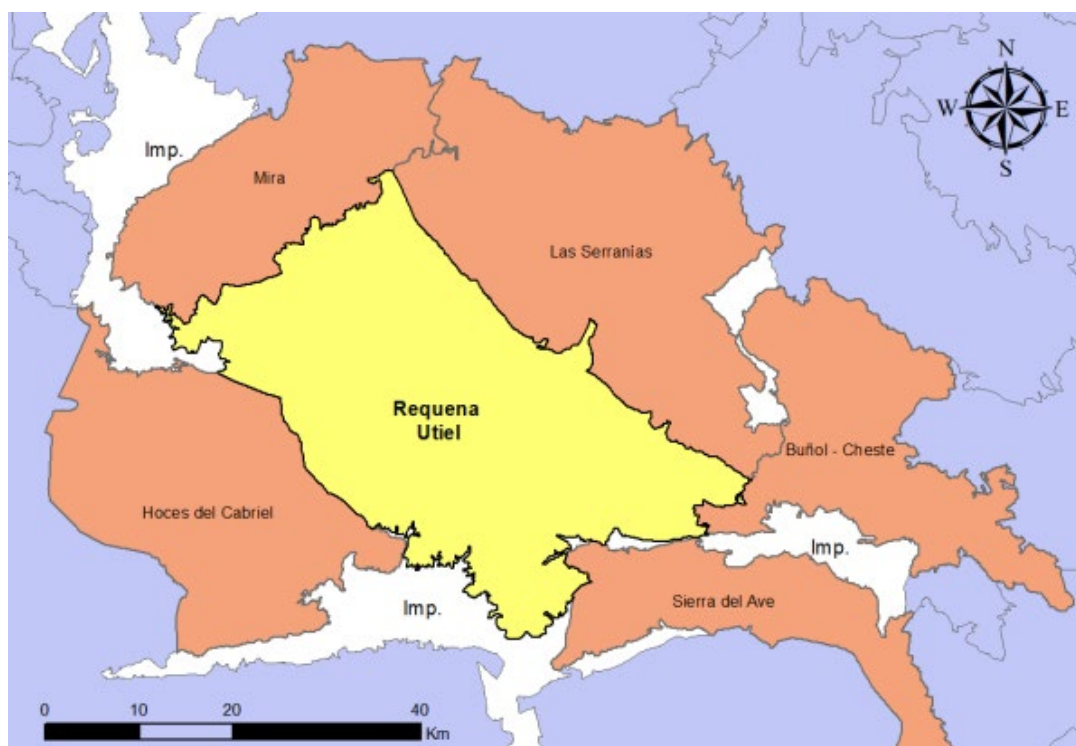


Figure 1. Requena-Utiel aquifer and its lateral limits

It was considered as internal boundary conditions for the Magro, the Madre and the Buñol rivers and the Torre ravine, as well as the recharge by infiltration of precipitation and by irrigation and pumping wells. The Magro river crosses the study area through the central part from the northeast to the southeast and it is the one that has the most significant influence on the aquifer. The Madre river is located in the northwest, the Torre ravine is in the northeast, and the Buñol river is in the southeast. A third type boundary condition was used to represent the rivers and after a calibration process, a conductance of  $100 \text{ m}^2/\text{day}$  was defined for the Torre ravine and the Madre river, to the Magro and Buñol rivers, a conductance of 12 and  $2.5 \text{ m}^2/\text{day}$  were defined, respectively.

The second type boundary condition was used to represent both the recharge and the pumping well. The recharge was considered heterogeneous in space by dividing the study area into 15 recharge zones based on the PATRICAL model (Pérez-Martín, M.A., 2005), and time, by following the dry and rainy seasons of the hydrological year. The pumping from wells was also considered variable in space and time, according to data available from the Júcar Basin authority.

Regions of similar hydrogeological behaviour have been defined for the spatial characterization of the hydrogeological parameters, resulting in five different domains. In the same way, these five domains have been thoroughly subdivided to create 20 subdomains. The value of hydraulic conductivity has a range between 0.02 and 19.5 m/day. Specific yield has a range between 0.0001 and 0.05, while specific storage varies between 0.3 and 0.1  $\text{m}^{-1}$ .

The numerical model performs a transient simulation during the period between the years of 1980 and 2016, with a monthly time discretization. The initial condition was defined from a previous steady-state simulation, representing the aquifer state from 1940 to 1979.

The numerical problem was solved by using the code MODFLOW 2005 (Harbaugh, A.W., 2005) through FloPy (Bakker et al., 2016).

The calibration was performed by adjusting model parameters manually and evaluating the difference between observed and simulated piezometric heads at ten measurement locations where time-series data were available.

### Description of the Surrogate Model

---

The idea is to use a machine learning algorithm to capture relationships between the piezometric heads in the monitoring points (targets) and the scenarios evaluated (features). The smart modelling process implemented can be summarized in six steps as follows:

The first step is to generate the data that will feed the algorithm to be trained. We selected 110 points along the study area, so that the entire aquifer was covered. These points were used as monitoring point of the piezometric head, then 110 targets were defined. The year, month, recharge, and pumping rate were selected as features. Since the basic numerical model previously described was built and satisfactorily calibrated, it served as a base for generating a

training dataset. For that, we kept all the model characteristics constant except recharge and pumping rate. The recharge rate was assumed to have an increment and a reduction of 30% (represented by a recharge factor ranging from 0.70 to 1.3) in relation to the average of the last ten years. It was assumed that the change in the recharge rate follows a linear function (increasing or decreasing) in time, with zero change for the first time-step (# 0) and a maximum change for the last time-step (# 432). Pumping wells were considered to have an increment and a reduction of 25% in relation to the average of the last ten years and it is applied directly to each time-step. It was generated 64 combinations of recharge and pumping rate. After that, the numerical model was performed for each combination between 2016 and 2052 (36 years), with a monthly time discretization (totalling 432 months), and the values of the piezometric heads were computed in the 110 monitoring points. In summary, for each model run, we obtained a dataset of 432 values of piezometric head, totalling a dataset with 27,648 data for each monitoring point. Figure 3 shows part of the generated dataset.

month	year	recharge	pumping	obs_point 1	obs_point 2	obs_point 3	obs_point 4	obs_point 5	obs_point 6	obs_point 7	obs_point 8	obs_point 9	obs_point 10
10	2016	0.7	0.75	731.17	766.29	728.46	773.34	748.91	733.35	735.34	783.12	768.91	755.51
11	2016	0.7	0.75	731.18	766.30	728.46	773.33	748.91	733.61	735.87	783.12	768.91	755.56
12	2016	0.7	0.75	731.19	766.31	728.46	773.33	748.91	733.56	735.94	783.11	768.91	755.57
1	2017	0.7	0.75	731.20	766.31	728.46	773.32	748.91	733.64	736.18	783.11	768.91	755.61
2	2017	0.7	0.75	731.20	766.32	728.46	773.32	748.91	733.62	736.25	783.10	768.91	755.63
3	2017	0.7	0.75	731.21	766.33	728.46	773.32	748.90	734.13	737.25	783.11	768.91	755.71
4	2017	0.7	0.75	731.22	766.34	728.46	773.32	748.90	734.27	737.82	783.10	768.91	755.73
5	2017	0.7	0.75	731.23	766.35	728.47	773.32	748.90	734.06	737.77	783.10	768.91	755.72
6	2017	0.7	0.75	731.23	766.36	728.47	773.32	748.90	733.77	737.40	783.09	768.91	755.71
7	2017	0.7	0.75	731.24	766.36	728.47	773.32	748.89	733.48	736.86	783.07	768.91	755.69
8	2017	0.7	0.75	731.25	766.37	728.47	773.32	748.89	733.28	736.36	783.07	768.91	755.69
9	2017	0.7	0.75	731.26	766.37	728.47	773.31	748.89	733.36	736.31	783.06	768.91	755.71
10	2017	0.7	0.75	731.26	766.38	728.47	773.31	748.88	733.70	736.82	783.06	768.91	755.75
11	2017	0.7	0.75	731.27	766.39	728.47	773.31	748.88	733.89	737.26	783.06	768.91	755.77
12	2017	0.7	0.75	731.28	766.39	728.47	773.31	748.88	733.80	737.25	783.05	768.91	755.76
1	2018	0.7	0.75	731.29	766.40	728.48	773.32	748.88	733.84	737.40	783.04	768.91	755.77
2	2018	0.7	0.75	731.29	766.41	728.48	773.32	748.87	733.80	737.40	783.04	768.91	755.77
3	2018	0.7	0.75	731.30	766.42	728.48	773.32	748.87	734.28	738.31	783.04	768.91	755.82
4	2018	0.7	0.75	731.31	766.43	728.48	773.33	748.87	734.41	738.82	783.04	768.91	755.83
5	2018	0.7	0.75	731.32	766.43	728.48	773.33	748.87	734.18	738.70	783.03	768.91	755.80
6	2018	0.7	0.75	731.32	766.44	728.48	773.33	748.87	733.89	738.27	783.02	768.91	755.78
7	2018	0.7	0.75	731.33	766.45	728.48	773.33	748.86	733.59	737.68	783.01	768.91	755.75
8	2018	0.7	0.75	731.34	766.45	728.48	773.33	748.86	733.38	737.13	783.00	768.91	755.73

Figure 2. Part of the generated dataset used for training the surrogate model

The second step is to define the best random split of the data set into training and test data, which will be used to evaluate the performance of the model. In our case, the best training and test results were obtained from 90% training and 10% test data.

The third step is to define a suitable algorithm and its hyperparameters. We have tested the performance obtained with AdaBoost (Freund & Schapire, 1997), XGBoost (Chen & Guestrin, 2016) and Random Forest regression (Breiman, 2001). Despite all of them being ensemble

methods, only Random Forest is natively multi-output, as required in our problem, so AdaBoost and XGBoost were adapted to handle multi-output regression problems. After comparing the performance of the tree aforementioned algorithms, we selected the latter, which is a supervised machine learning algorithm for building a predictor ensemble with a set of decision trees (forest) that grow in randomly selected sub-samples of the dataset (Biau, 2012; Breiman, 2001; Cutler et al., 2012).

By using the scikit-learn library in Python (Python Core Team, 2015), it was conducted a sensitivity analysis to define the best hyperparameters to be used in the Random Forest regressor: the number of trees in the forest = 60, the maximum depth of the tree = 30, the minimum number of samples required to split an internal node = 2, the number of features to consider = 0.75. We used the default values of all other hyperparameters as defined in scikit-learn.

The fourth step is to train the regressor by feeding it with 90% of the dataset generated in the first step: a data set with 24,883 data.

In the fifth step, the performance of the fully trained surrogate model is evaluated on the testing dataset previously defined in step 2. Additionally, k-fold cross-validation with  $k = 5$  is also performed to evaluate the model on a limited data sample.

Finally, in the sixth step, the regressor is used to predict. The user must provide as input data: month, year, change in the recharge (increase or reduction), and change in the pumping rate (increase or reduction). As a result, the model will return the interpolated piezometric head for the entire aquifer based on the 110 monitoring points. The interpolation was done in Python by using the radial basis function method with the thin plate spline method.

### Evaluation of the Performance

---

The performance of the surrogate model was obtained by evaluating the regression score and the mean square error for testing data. Cross-validation was also performed as an alternative method to estimate the model skill. As the surrogate model is used to replace the numerical model due to its high computational cost, it is also important here to evaluate the time needed to obtain a response when using the numerical or the surrogate models. Figure 3a shows the

mean regression score obtained by using Random Forest (RF), AdaBoost (AB) and XGBoost (XB) algorithms, while Figure 3b shows the mean square error over 64 scenarios.

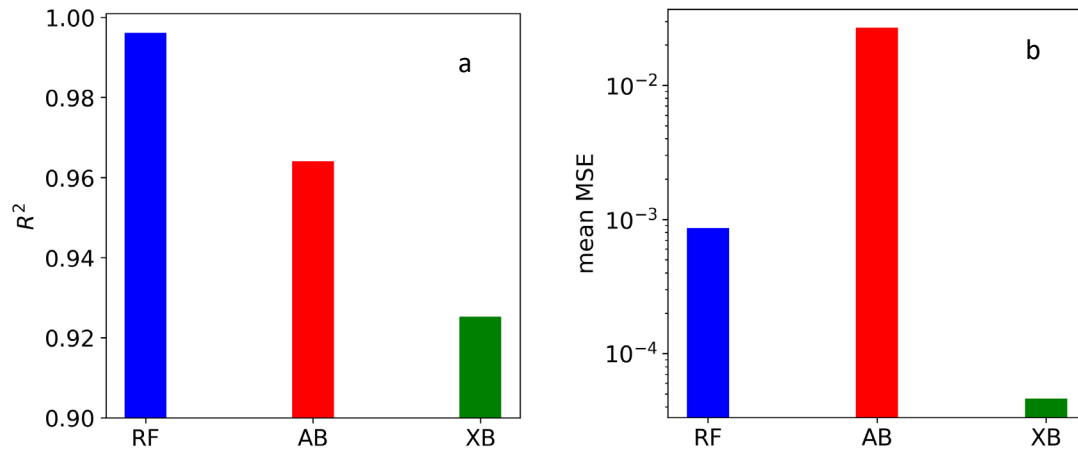


Figure 3a. Mean regression score obtained by using Random Forest (RF), AdaBoost (AB), and XGBoost (XB); 3b. Mean square error over 64 scenarios.

Results shown that Random Forest, AdaBoost, and XGBoost performed similarly and presented high accuracy of the models against the training data. Table 1 shows the results of the cross-validation, and we can see that the good performance is confirmed for the three algorithms.

Table 1. Mean cross-validation scores for each fold

Scores	fold1	fold2	fold3	fold4	fold5
RF	0.86	0.89	0.96	0.93	0.93
AB	0.68	0.81	0.88	0.88	0.79
XB	0.76	0.83	0.91	0.86	0.85

Figure 4 shows the mean CPU time (in seconds) necessary to obtain the response. As mentioned before, Random Forest not only presented high accuracy, as well as the other methods, but also the computational time was reduced in 36 times when compared to the time required by MODFLOW.

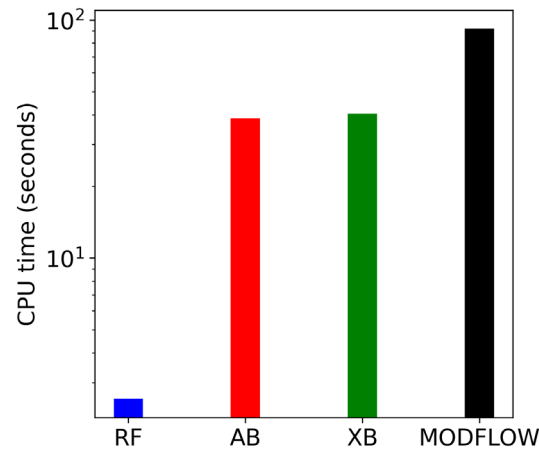


Figure 4. Mean CPU time required to calculate and get the piezometric head values

Due to the good performance and computational time obtained by using Random Forest, this is the model chosen to build our surrogate model. Figure 5 shows the piezometric levels obtained with MODFLOW (test data) and with the surrogate model.

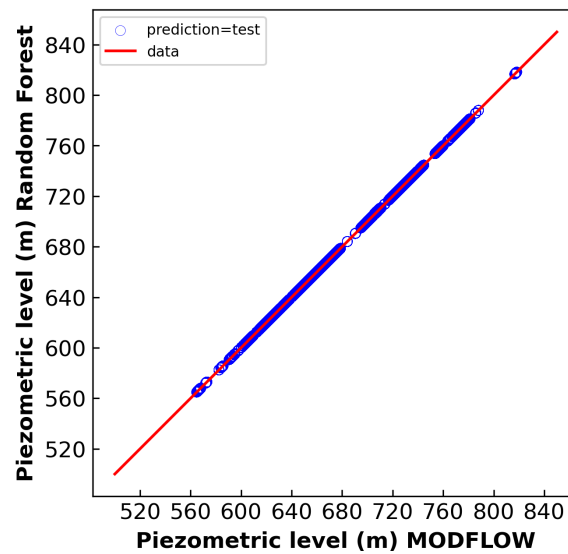


Figure 5. Piezometric heads obtained with MODFLOW (test data) and with the surrogate model (Random Forest)



## 2.2. Tympaki (Greece)

### Objectives of the Surrogate Model

The goal of this study is to use a groundwater numerical simulation model to obtain the water table dynamics under hydrological scenarios. Then, a space-time regression Kriging method was chosen to establish a surrogate model for the numerical simulation model. The established surrogate model is used to put forward the annual control index of the groundwater table based on a certain control index of the groundwater exploitation amount. It is expected that the proposed method can improve the management of groundwater in the basin and satisfy the demands of the relevant management authorities.

### Description of the Complete Numerical Model

The study area has a width of about 12.5 km and a length of about 9.1 km. There are 371 pumping wells which were grouped into 20 pumping locations by using the K-nearest neighbors and each group was represented as one pumping well by using the Median Center method, which identifies the location that minimizes overall Euclidean distance to the features in a dataset (Figure 6). The pumping rate of each group is the total pumping rate of all the wells constituting the group in  $\text{m}^3/\text{d}$ . The pumping rates are imported in FEFLOW as time-series with the values being different for the wet and dry seasons.

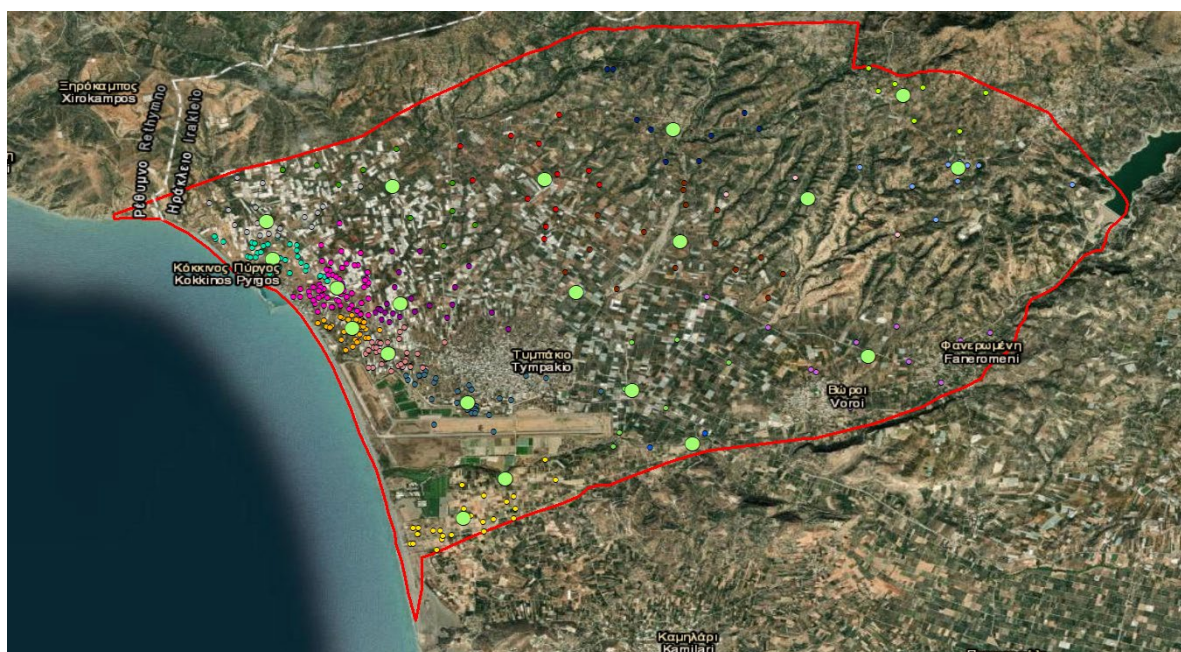


Figure 6. All the wells along with the representative ones for each group

The discretization of the unconfined aquifer was applied using a triangular finite element mesh which consists of 11,877 nodes and 15,340 elements. There are 2 layers and each one of them has 7,670 elements and 3 slices with 3,959 nodes for each slice. The depth of the model comprises 130 m deep from the sea level for the unconfined aquifer. The data for the hydraulic conductivity were extracted from the Decentralized Administration of Crete and they were set for the axis  $x'x$  and  $y'y$ . For  $z'z$  the hydraulic conductivity was 10% of the value of  $x'x$ . The pumping wells as considered in the model are depicted in Figure 7.

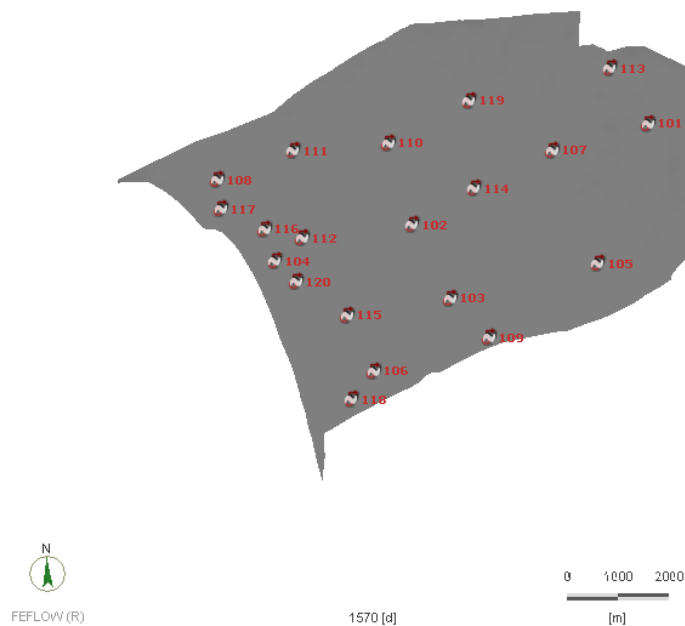


Figure 7. Pumping wells spatial distribution

The calibration – validation process was conducted as follows: In the area of Tympaki there are 6 observation wells that are distributed in the study area, as shown in Figure 8. The hydraulic head data are used as time series and the period for each well is different. The time series period for the precipitation, observation wells and pumping wells are available for the years 2004-2014. For the precipitation, the data of 1 station is used. In sake of computational time, a mean precipitation was used with a step of 10 days and the input time series is in units of m/d. The data from 04/2004 until 04/2009 are used for calibration and the rest for validation. During the validation period, the field measurements at the observation wells were conducted in random dates so there are periods with no data available at the observation wells. The mean error for the validation period is 6.4 meters.



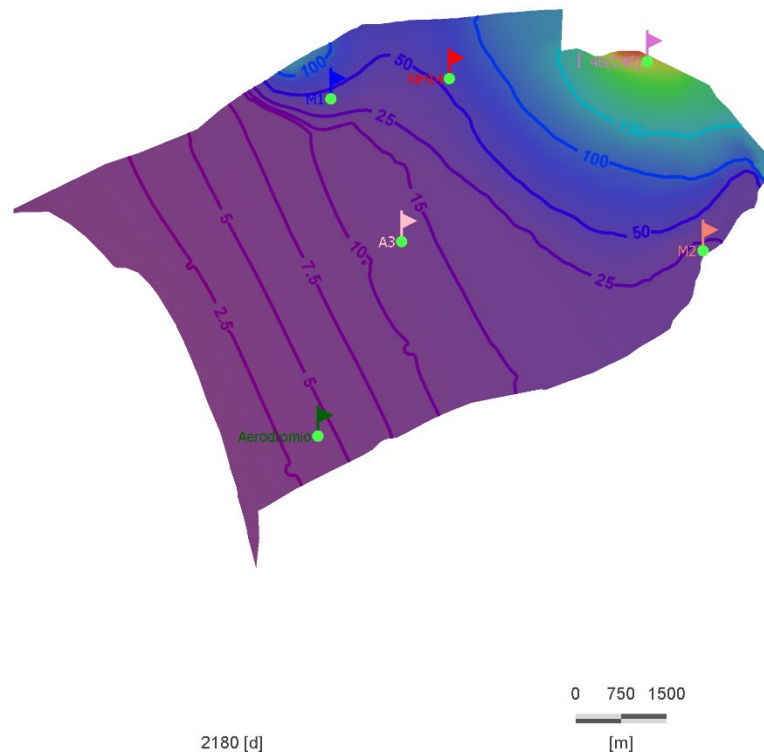


Figure 8. Observation wells with calibration – validation data available

For the model of the Tympaki area, a first-type flow boundary condition was used along the coastline, where the hydraulic head was set at 0 m. Also, a second-type boundary conditions were set at the north boundaries of the study area. Those boundary conditions are connected to the precipitation so there is a fluctuation to the hydraulic head that is relative to the rainfall. The observation wells that are used in the pumping scenarios were set to monitor the saltwater intrusion zone. As it appears in Figure 9, the intrusion zone is estimated to occur between the coast line and at 5.65 meters above the sea level (at the end of the calibration period), by using the Ghyben – Herzberg relation and considering the depth of the deepest pumping well in the area (226 m below the sea level). The simulation runs are applied for a ten-year period from 01/04/2010 until 31/03/2020, by using the available precipitation data, as well as time series for the pumping rates. For the values of pumping rates obtained from the licences of water use, the results of the model are depicted in Figure 10 and Figure 11 and the values of the hydraulic heads in the observation wells in Figure 12.

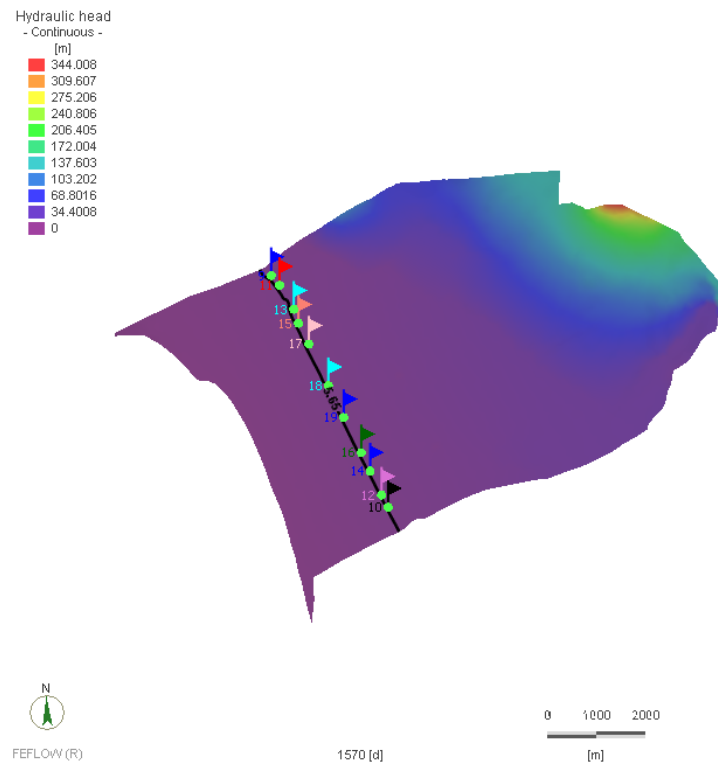


Figure 9. Salt water intrusion zone 2009

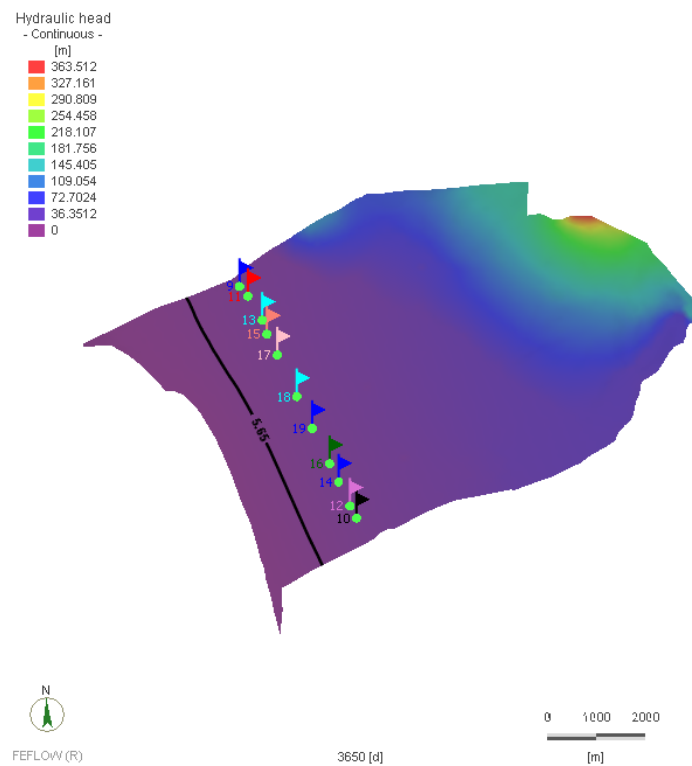


Figure 10. Simulation results wet period October 2019- March 2020

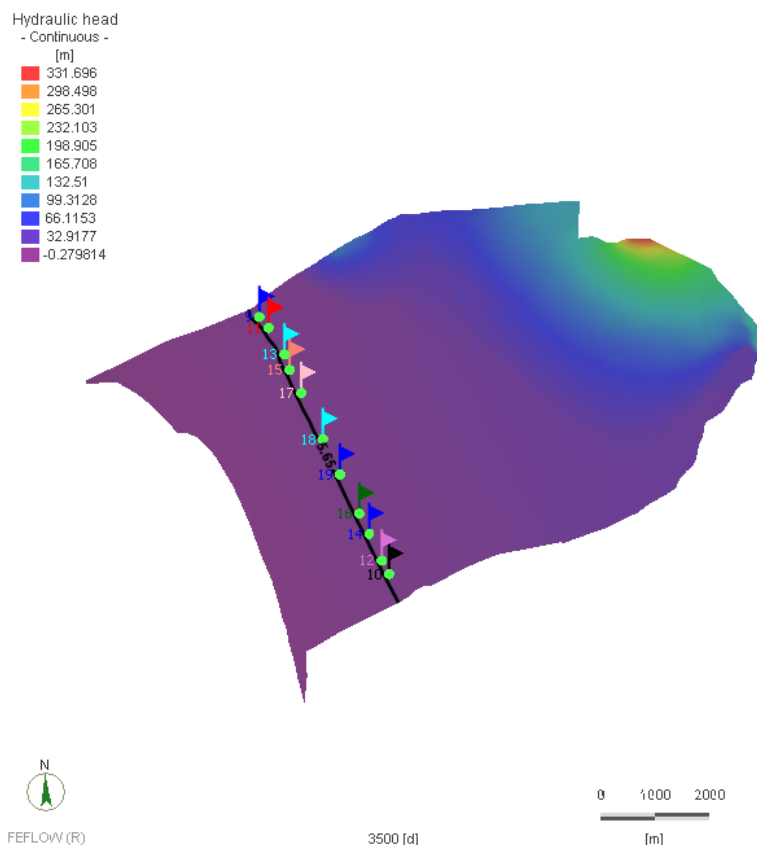


Figure 11. Simulation results dry period April 2020-September 2020

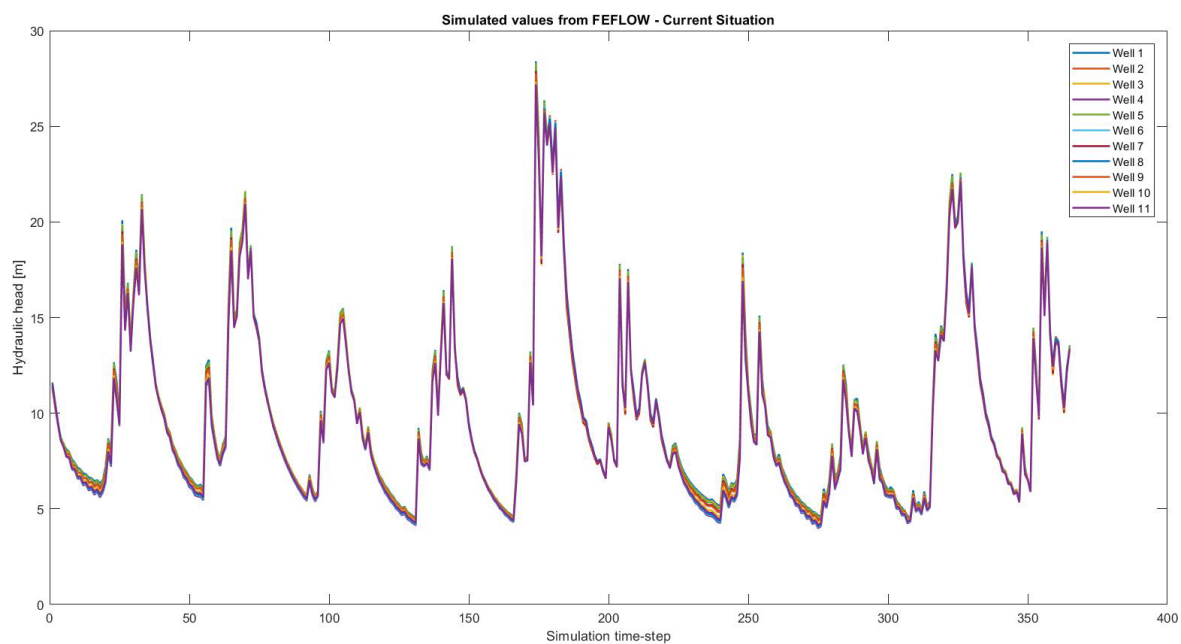


Figure 12. Simulated hydraulic heads at the observation wells

## Description of the Surrogate Model

---

Spatiotemporal geostatistical analysis of groundwater levels is a significant tool for groundwater resources management. This work presents a valid spatiotemporal geostatistical model for the groundwater level variations of the Tympaki aquifer in Crete, Greece. The main goal of space–time analysis is to model multiple time series of data at spatial locations where a distinct time series is allocated. The time variable is considered an additional dimension in geostatistical prediction. Using spatiotemporal geostatistics, the groundwater level dataset can be usefully exploited in order to identify the spatiotemporal behaviour of the aquifer and to obtain useful information regarding the space–time data correlations for more accurate space–time predictions (Varouchakis 2017; Varouchakis and Hristopulos 2019). Space–time geostatistical analysis involved the following steps: (1) space–time variogram calculation, (2) application of space–time regression kriging (STRK by means of elevation) for prediction, and (3) estimation of prediction accuracy. The goal of this approach is to accurately map the aquifer level at variable time-steps using joint space–time information. The proposed model applies the STRK methodology using joint space–time covariance functions. A space–time experimental variogram is determined from the groundwater level time-series between the hydrological years 2004 and 2015 at 11 sampling stations bi-annually (Figure 13). Elevation was considered as a secondary variable because according to a test provided by Haitjema and Mitchell-Bruker (2005) it was found that it consists a direct replica of the water table. The experimental spatiotemporal variogram of the fluctuations was successfully fitted by the product–sum model using a Matérn spatial and temporal function (Figure 13). STRK was used to predict the bi-annual groundwater level at each sampling station from 2016 to 2020.

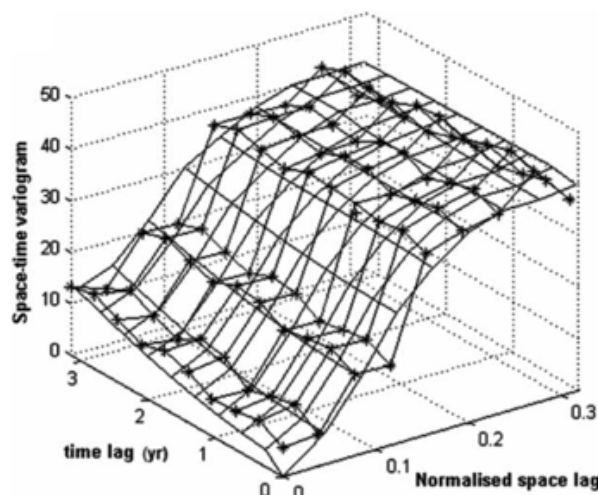


Figure 13. Space–time variogram fit (stars) using the product–sum model

### Evaluation of the Performance

The proposed surrogate model efficiency was assessed by a validation procedure that considered the period 2016-2020. The cross validation was initially applied for the 11 observation wells. Validation results (Table 2) provided low prediction errors that range from 0.95 to 1.45 m, therefore, maps of groundwater level spatial distribution in the area were developed to assess the aquifer spatiotemporal variability. The predicted groundwater levels contours were compared with those from the numerical model. In addition, a second validation set of groundwater levels was available for the hydrological year 2019-2020 at 53 locations, being 2020 the last modelling year. These observed groundwater levels came from the registration of private wells during the hydrological year 2019-2020. The cross-validation analysis provided a MAE of 1.75 m. The latter is higher than the one based on the 11 wells for the period 2016-2020 due to the greater spatial distribution of the monitoring points, especially for those close to the boundary zones. However, still the error is satisfactory compared to the range of the groundwater level in the area.

Overall, the surrogate model results based on STRK (Figures 14, 15) agree with those of the numerical model (Figures 10, 11) and they consist a reliable alternative for the modelling of the aquifer levels. The differences between the two modelling approaches are located at the boundary zones due to their different principles on functionality and application. The proposed surrogate model results can be further improved from the enrichment of the available datasets with groundwater level observation locations. This work demonstrated that space–time

geostatistics can successfully represent the spatial dynamic behaviour of an aquifer when the space–time dependencies are appropriately modelled, even for a sparse dataset.

Table 2. Average STRK prediction statistical measures for using the product–sum space–time variogram in terms of ME, mean error; MAE, mean absolute error; MARE, mean absolute relative error; RMSE, root mean square error;  $R^2$ , coefficient of determination.

	MAE (m)	ME/BIAS (m)	MARE	RMSE (m)	$R^2$
2016	1.10	0.18	0.12	2.75	0.90
2017	0.95	0.08	0.11	2.14	0.91
2018	1.25	−0.25	0.13	3.41	0.88
2019	1.45	−0.32	0.15	3.80	0.88
2020	1.24	0.20	0.13	3.34	0.88

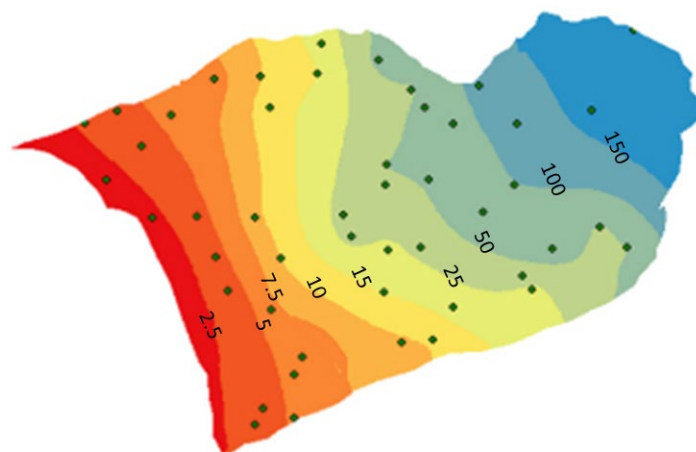


Figure 14. Groundwater level spatial distribution, meters above sea level, for the wet period of October 2019–March 2020

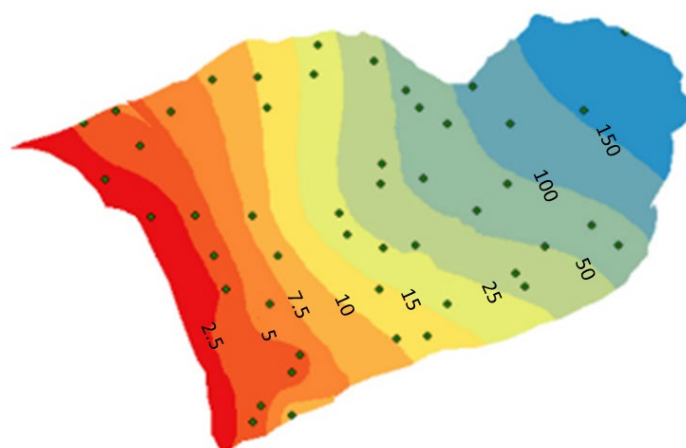


Figure 15. Groundwater level spatial distribution, meters above sea level, for the dry period of April 2020-September 2020

### Self-Organizing Maps Approach

---

In this approach the main dataset consists of 341 observations for the year 2021 that include X-Y coordinates and hydraulic head value. The aim of this work is to define sub-datasets which will improve the results of Ordinary Kriging. The processes of the proposed methodology is as follows: performing OK in the whole dataset, exploration of different pre-classification arrangements (topologies) and assessment of performance of OK for each topology. This rudimentary analysis of the methodology is further explained in detail below. The first step of the algorithm consists of reading and formatting the necessary data. The data are organized in a table format to facilitate computations in MATLAB. Formatting it in coordinates and hydraulic head values, which in general are the inputs for both SOM and OK. The initial topology is set to 1x1 which will constitute the base line for assessment for all different topologies. The SOM algorithm constitutes the pre-classification part of the methodology. The inputs of the SOM model are the X-Y coordinates and the hydraulic head value. The outputs are the same values, but classified in clusters. This selection ensures that classification will be done based on the location of the observations in the field and the different hydraulic properties or conditions that are correlated to the hydraulic head value. This use of SOM classifies each observation to a single cluster, and OK is applied to each cluster separately. Although there is a possibility of overlap between OK predictions, this is only for small areas at the borders of each cluster. It is worth noting that an underperforming cluster, relative to the initial topology, will not affect a

cluster that produces acceptable or improved results, over the initial topology. Each different combination of clusters constitutes a topology, for example the first topology that Kriging will be performed on is 1x1, which means a single cluster, i.e., the whole dataset; thus, SOM is not necessary for this topology. Adding another cluster, produces two additional possible topologies, namely 1x2 and 2x1. Since it is possible that the classification will produce a cluster with different observations included in each one. Both will be explored. In topology 2x2 such problem does not exist. In 2x3 and 3x2 the process will be the same as above. In conclusion the SOM algorithm will either classify correlated observation with each other or exclude non-correlated observations and overall refining the variogram calculation and the inputs of OK.

Topology's 1x1 performance was deemed adequate, despite having high error score. OK technique can describe the geohydrological conditions of the case study, but by classifying the observations, OK can produce more accurate results. The use of SOMs can greatly improve predictions even in simple topologies like 1x2 and 2x1. Small differences can greatly affect the result of Kriging as it is apparent when comparing the two topologies. That signifies that topology configuration is important and related to the physical problem at hand. Topologies 1x2 and 2x1 divided the study area in two groups based on the location of the observations and the change of linear trend of hydraulic head value. In topology 2x2 subgroups were subdivided with further detail while incorporating the geohydrologic properties of each group. In topologies 2x3 and 3x2 the groups were more detailed, such division had mixed results. In topology 2x3 the model was strangulated and did not produce acceptable results for one cluster, whereas topology 3x2 provided the most accurate and improved results compared to topology 1x1. Topology 3x2 (Figure 16) based on all metrics was elected to be the most fitting for this case study (Figure 17). In cluster 1 of said topology, the correlation coefficient was approaching zero but that indicated that the cluster can be described only by the deterministic linear trend. The low correlation coefficient score though does not affect the robustness of the prediction since all other error scores outperform the initial topology. Six groups were defined for the optimum description of the geohydrologic conditions of the case study constructing the relative variograms (Figure 18). The first group is located in the northern-west part of the study area, upon the porous aquifer with 25% infiltration. The second group is located in the cross section of the 3 porous formations in the middle of case study. The third group consists of the coastal front with the most intensive agricultural activity. The fourth group is located in the



northern part of the case study which is affected by the river discharge. The fifth group is located in the mainland in a cross-sectional area of aquifers in high altitude. The final group is at the coastal front but is differentiated by the other coastal group because of different morphology. The clustering done by SOM provided detailed granularity in the grouping with seemingly reductive inputs. The coordinate inputs were most prevalent in the influence of the grouping in topologies 1x2 and 2x1. In other topologies, in which there was more room for diversification the hydraulic head value affected greatly the grouping results. The explanation behind that is 2-fold, firstly as a numerical input the SOM algorithm grouped observations in close proximity to each other and with similar hydraulic head values. Secondly, the hydraulic head value is strongly correlated to secondary parameters like hydraulic conductivity or altitude. Altitude is easily extracted as information but hydraulic conductivity measurements are few and include uncertainty. Thus, hydraulic head as an input contains secondary information that the SOM algorithm can utilize to perform an improved grouping. In conclusion, the pairing of SOM-enhanced OK in each cluster of data can produce a combined map of the hydraulic head spatial variability (Figure 19) of high definition and accuracy compared to a simple OK technique. The methodology proposed is generic which means it can be applied to different case studies by only altering the inputs as presented above and testing different topology configurations. This work produces spatial predictions, the future development of the proposed methodology aims to incorporate the temporal aspect of the geohydrologic conditions in the case study.

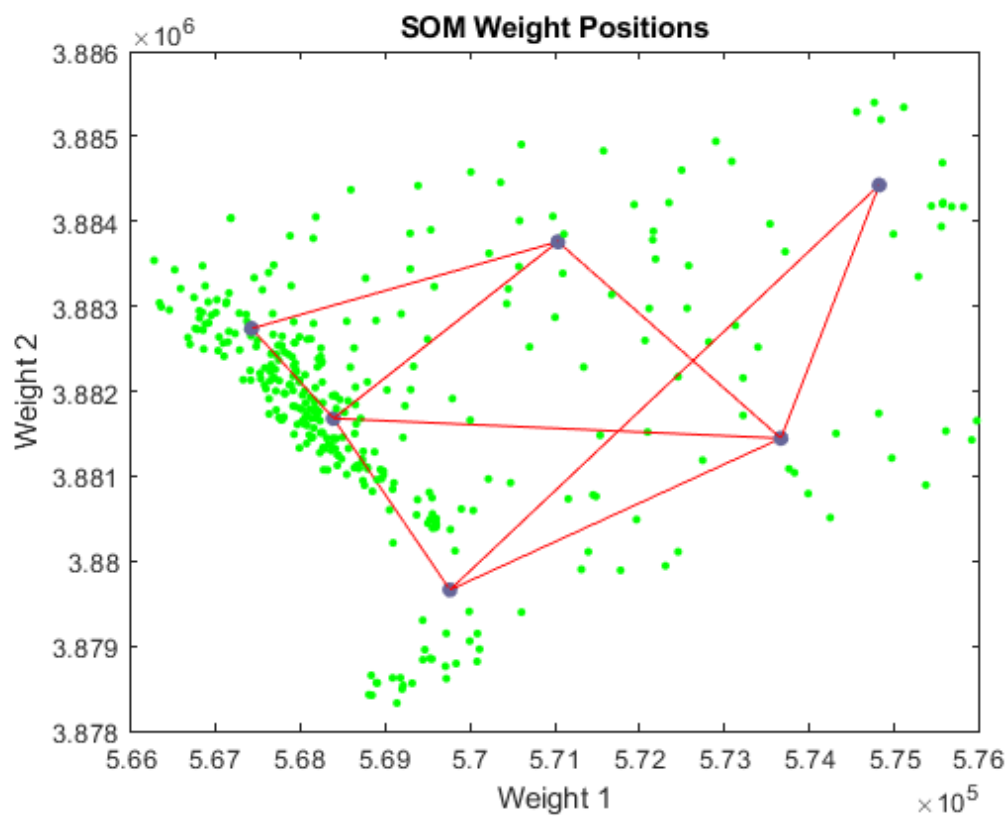


Figure 16. Spatial distributions of observations and their related cluster

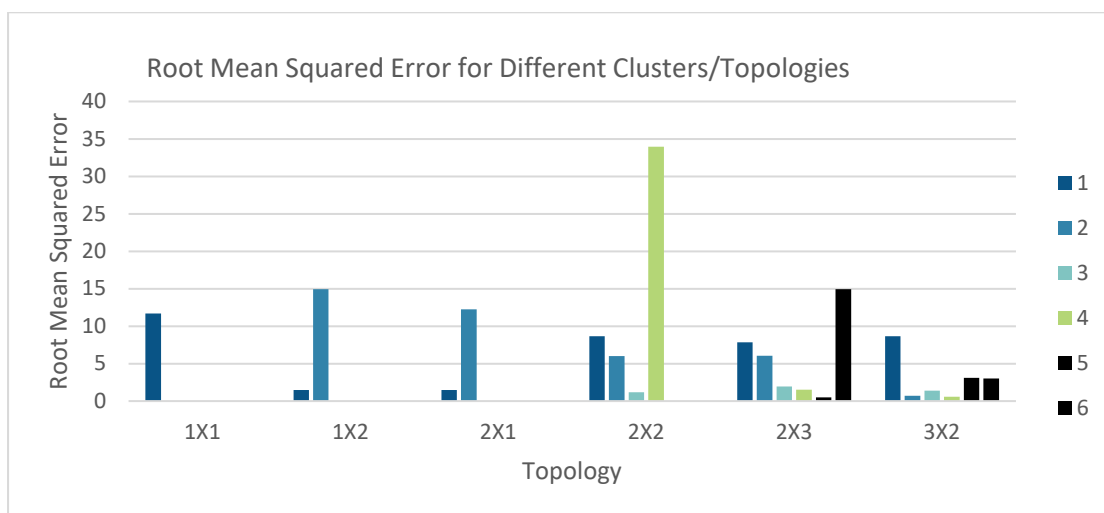


Figure 17. Root Mean Squared Error for Different Clusters/Topologies

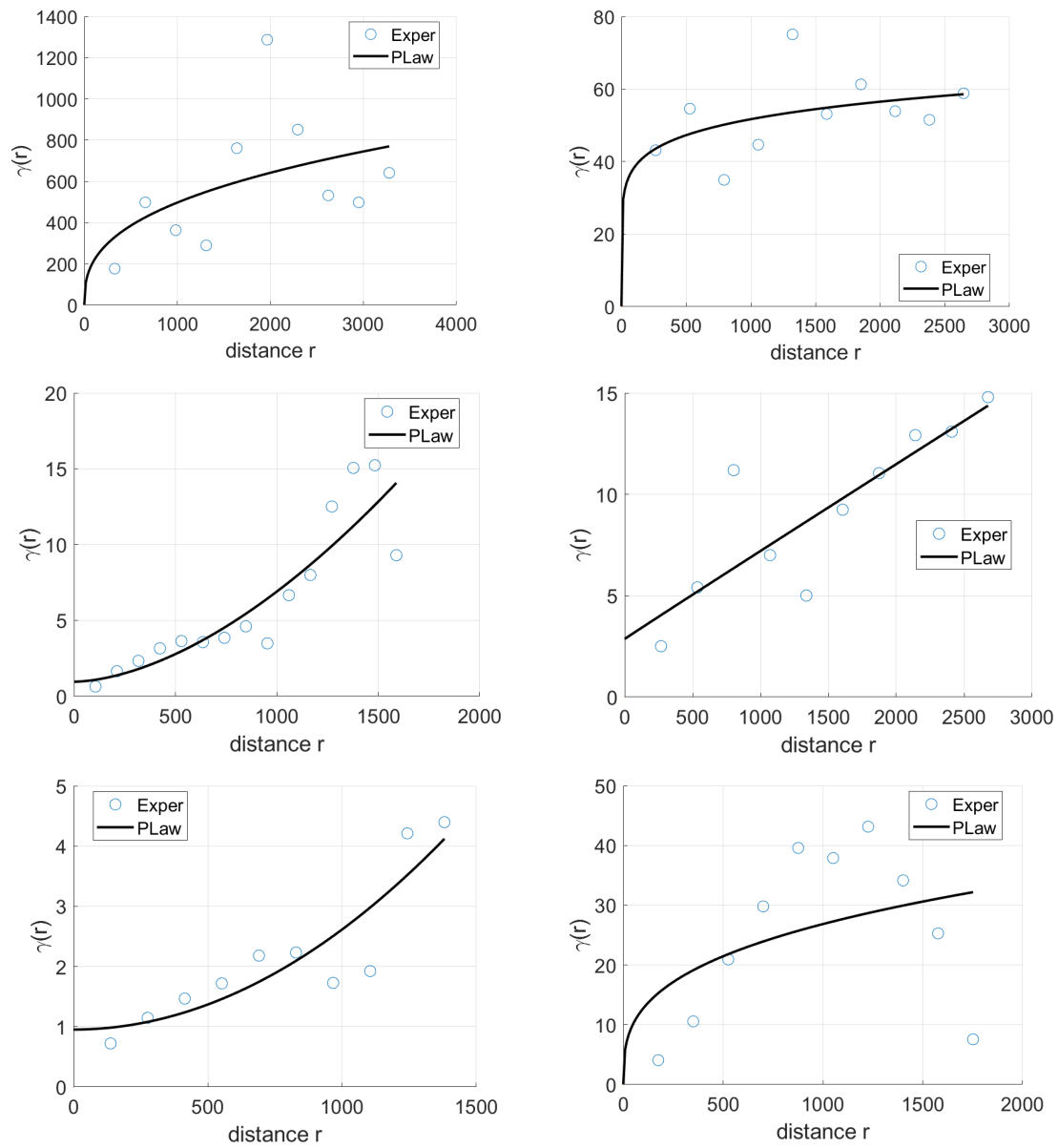


Figure 18. Variograms for cluster 1-2,3-4,5-6

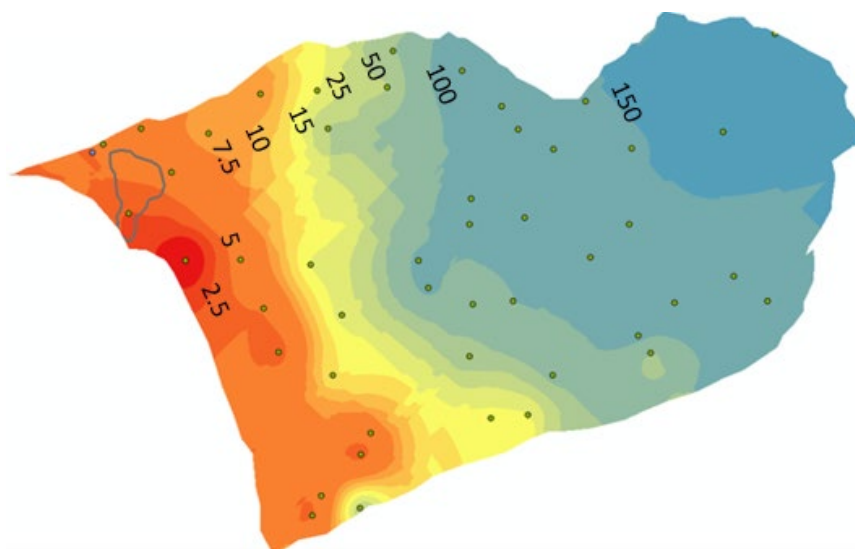


Figure 19. Spatial variability of hydraulic head (meters above sea level) in the area of Tympaki using SOM-OK approach

## 2.3. Konya (Turkey)

### Objectives of the Surrogate Model

The Konya closed basin is located in the central Anatolian plateau with an area of about 50,000 km<sup>2</sup>. The surface elevation ranges from about 900 m in the central portions of the basin to 3400 m along the Taurus Mountains which form the southern boundary of the basin (elevation data from General Directorate of Mapping of Turkey) as shown in Figure 20. The basin has a population of about 3.2 million and is characterized by a high level of biodiversity (Yilmaz et al., 2021). The basin has variable climate with Mediterranean climate in the south and dry and cold climate in the north. The mean annual precipitation is about 380 mm, ranging from about 290 mm in the central dry regions to about 650 mm in the southern mountainous boundary of the basin (Figure 21).

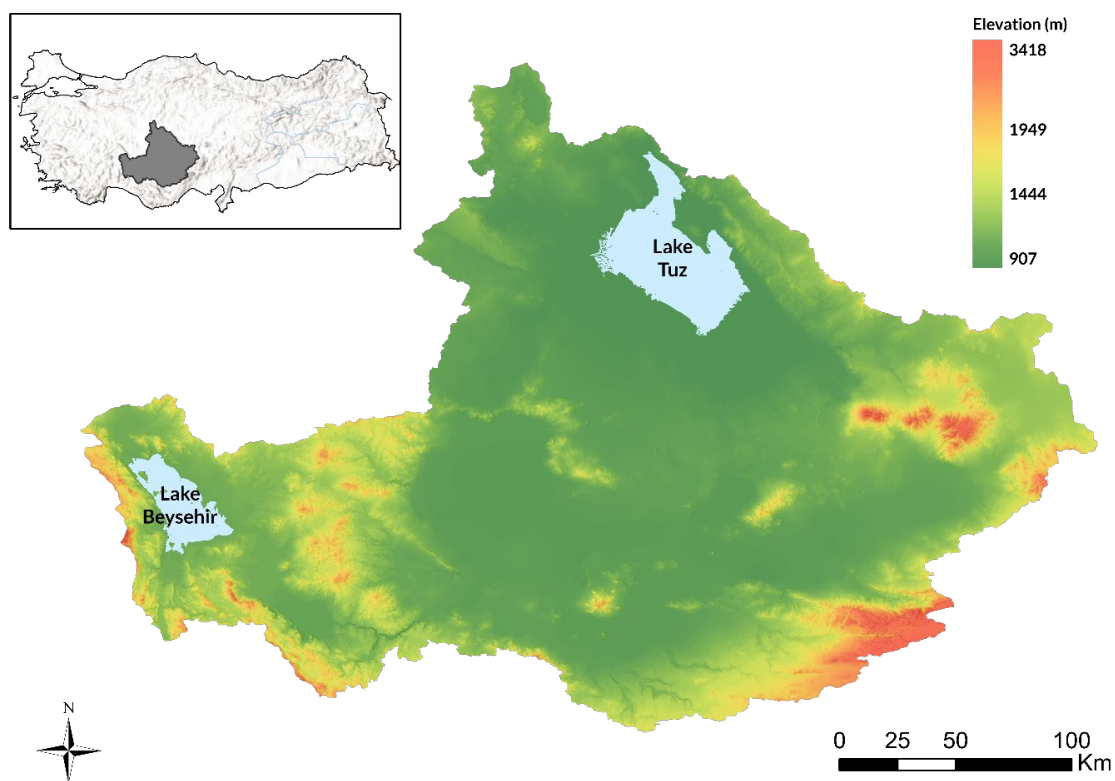


Figure 20. Location Map and Surface Elevation of Konya Closed Basin

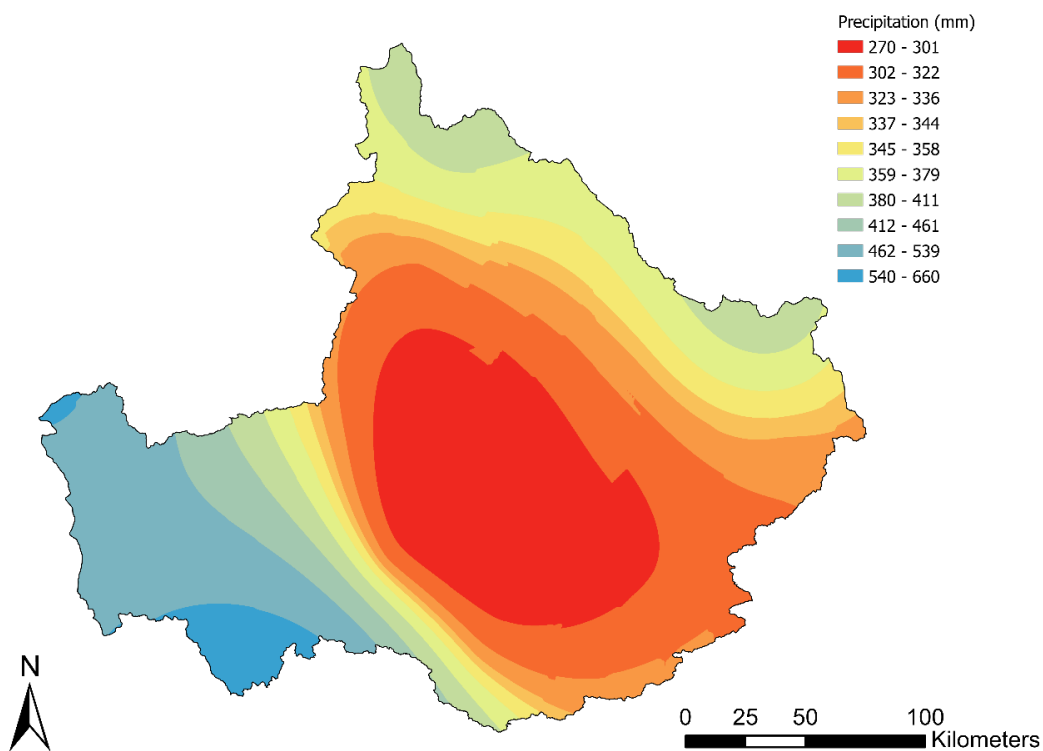


Figure 21. Average Annual Precipitation of Konya Closed Basin (1970-2020)

The Konya basin is one of the major agricultural regions of Turkey with more than 50% of the plain surface area used for agriculture as shown in the satellite land use map for year of 2018 (Figure 22). With no rivers or streams crossing its boundaries and precipitation concentrated in the winter months, agricultural activities rely heavy on groundwater resources. Despite the semiarid climate of the basin, water-intensive crops are cultivated in large portions of the basin. Especially in the last two decades, there has been a gradual change from traditional wheat farming to more profitable water-demanding crops such as sugar beets and maize (Yilmaz et al., 2021).

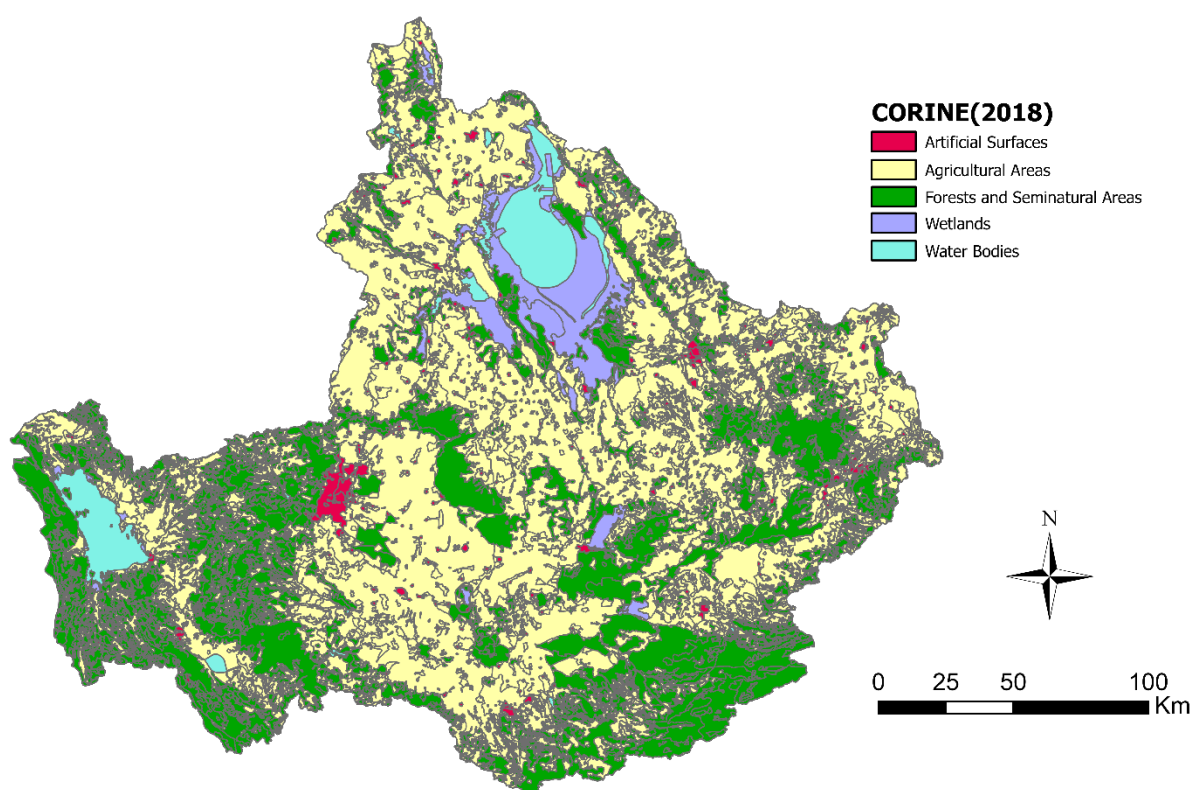


Figure 22. Satellite land use map of Konya Closed Basin for year of 2018

As a result of the extensive agricultural activities within the basin, groundwater levels have been steadily declining. This decline has placed significant pressure on the agricultural sector within the basin. To achieve a more sustainable use of groundwater resources in the basin, a hydrogeological model is being developed as part of Work Package 4 of the InTheMED project. The goal of this model is to estimate the net recharge over the basin which will help in the

management of the groundwater resources. The model is also used to assess the impact of different irrigation practices and climate change on the groundwater resources of the basin.

The purpose of the surrogate model is to provide a rapid, efficient and easy to use alternative to the detailed physics-based numerical hydrogeological model. The surrogate model, which is based on the artificial neural network method, will be used to reproduce the spatial historical groundwater head decline in the aquifer and assess the impact of various irrigation and climate change scenarios on the groundwater resources of the basin.

### **Description of the Complete Numerical Model**

---

UZF Package coupled with MODFLOW-2005 was used to develop a regional model that simulates the unsaturated-saturated groundwater flow over the entire basin. UZF simulates unsaturated flow based on the kinematic wave equation, a simplified version of Richards' equation, whereas MODFLOW simulates three-dimensional finite-difference groundwater flow. Coupling between unsaturated and saturated flow simulation is achieved as follows: for each time step, MODFLOW provides the location of the water table which acts as the lower constant pressure boundary of the UZF model, while the UZF model uses the surface water application (precipitation and irrigation) and evapotranspiration to compute the net recharge into the aquifer (Harbaugh, 2005; Niswonger et al., 2006).

The model domain covers the entire area of the Konya closed basin. No-flow boundary conditions were imposed along the outer model boundaries. Horizontally, the model domain is discretized into 10 km by 10 km uniform square grid (a total of 1015 cells). The initial head data in the model were defined based on the January 2,000 observed groundwater level data. The UZF module solves the kinematic flow equation for each of the model's active cells based on the temporal and spatially variable surface water application and evapotranspiration.

The model simulations extended for a period of 20 years, starting from Jan 1, 2000 to year Jan 1, 2020. The 20-year horizon was divided into 240 monthly stress periods. The time steps used for simulating the groundwater flow was equal to 1 day. Precipitation was determined from 18 meteorological stations covering the entire basin. Monthly precipitation data were defined in the model. Simple kriging was used to estimate the transient precipitation distribution over



the entire domain. Figure 23 gives the spatial distribution of the monthly precipitation for selected months/years.

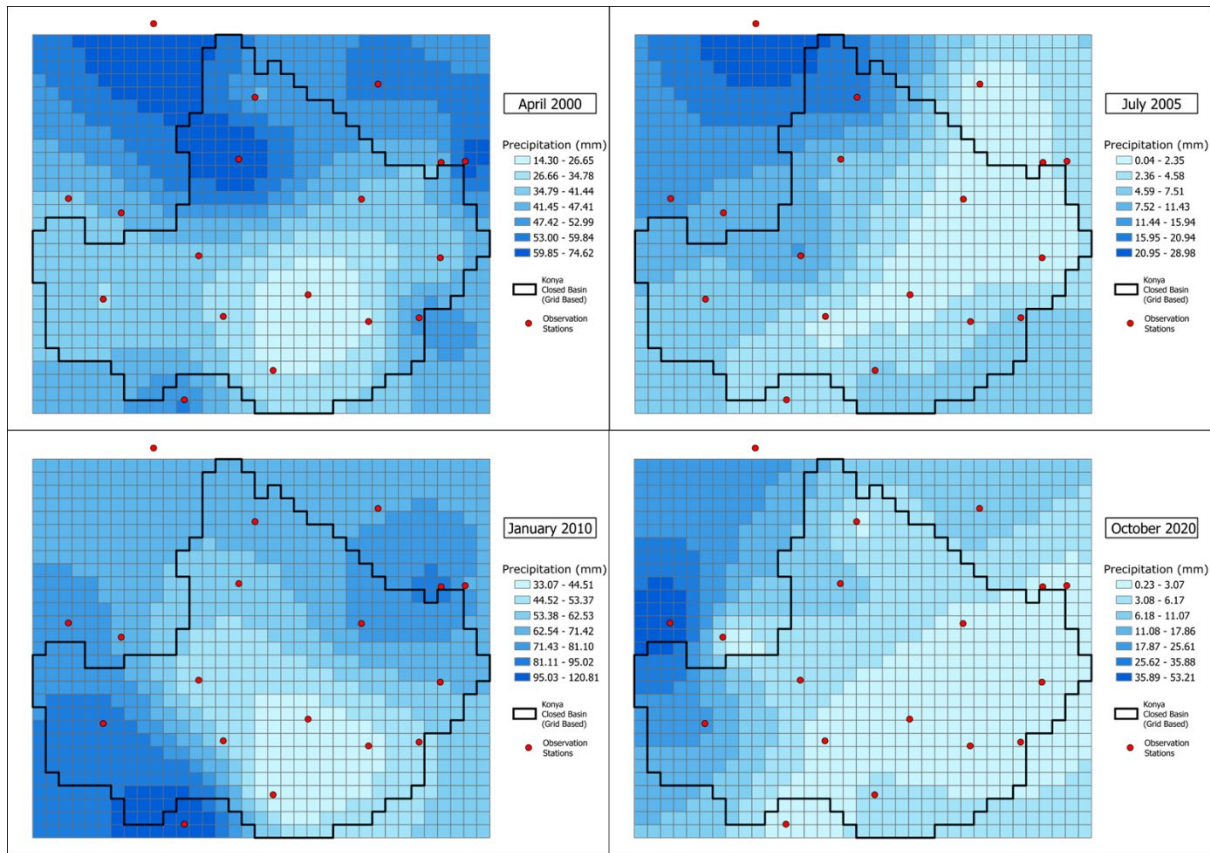


Figure 23. Monthly Precipitation Distribution over the Konya Closed Basin for selected year/months. Dots show location of available meteorological stations

Soil maps and well logs of the top soil indicate that the soil is mostly silty loam. In the model, the permeability and van Genuchten parameters of the soil are defined based on soil type and direct measurements of the water retention properties of collected soil samples. Geologic maps and well logs developed by the State Hydraulics Works (Devlet Su İşleri, DSI) were used to define the hydraulic conductivity of the aquifer system. DSI carried out a series of pumping tests with drawdown monitored at a total of 78 points. The hydraulic conductivity distribution over the entire domain was estimated using ordinary kriging. Figure 24 shows the spatial distribution of the hydraulic conductivity. The thickness of the aquifer was interpolated based on available well logs. Wherever the bottom of the aquifer was not reached, the bottom elevation was defined equal to the bottom of the well logs.



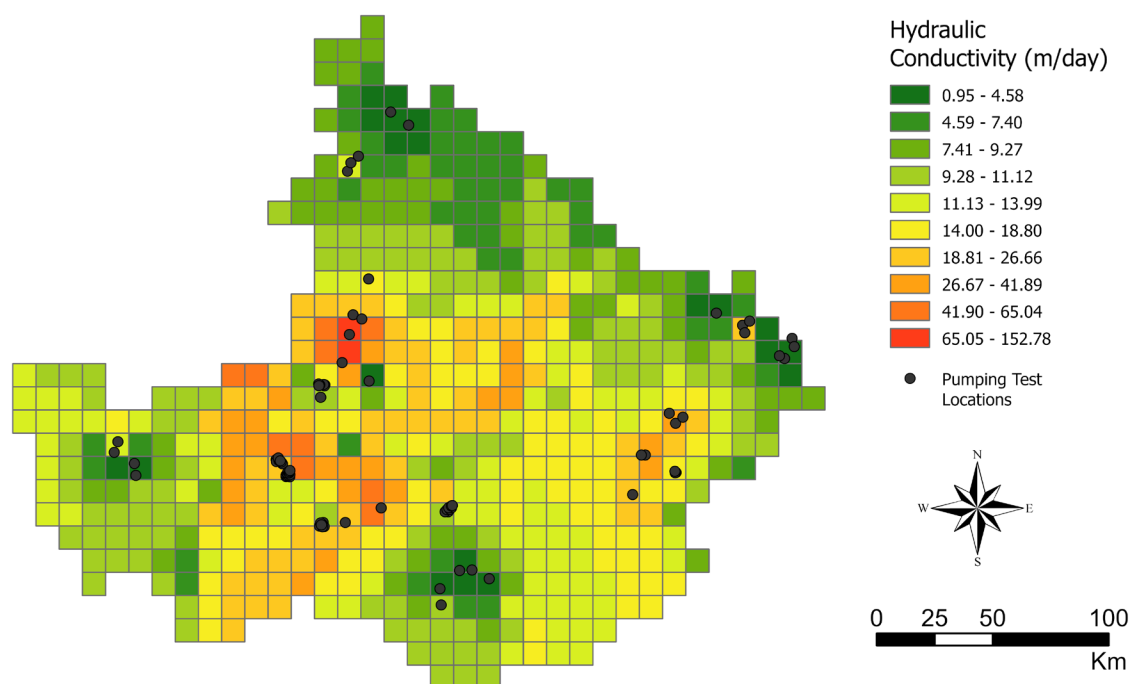


Figure 24. Hydraulic Conductivity of Konya Closed Basin

Given the large number of unmetered wells in the Konya Plain, it was not possible to directly estimate groundwater extraction rates. For this purpose, irrigation water demand was estimated indirectly from (i) historical crop production for individual townships (TUIK, 2020), (ii) recommended irrigation schedules for the area of Konya for different crops (TAGEM, 2017), (iii) irrigation efficiencies and (iv) land use satellite maps (Copernicus Land Monitoring Service). Historical irrigation efficiencies were defined based on available reports; it is generally observed that enhanced irrigation systems (drip and sprinkle systems) were gradually installed in the Konya plain starting from year 2010. To spatially distribute water demands, groundwater extraction rates for each model grid were defined as the difference between the irrigation water demand within that grid and the actual precipitation. This calculation was performed at monthly basis for the 20-year model duration. Potential evapotranspiration rates were defined based on climate data and land use maps on a monthly basis.

The calibration target was the historical monthly groundwater level data at various monitoring wells covering the entire model domain. The main calibration parameters were the spatial

distribution of the hydraulic conductivity, as well as irrigation efficiency and groundwater extraction rates which are associated with the highest level of uncertainty.

Figure 25 compares the simulated and observed monthly heads at all observation wells. Only observation wells with at least 20 years of data are shown in this figure. In general, the agreement is good with the simulated water trend close to the observed water trends. The simulated heads also show the seasonal variation in the water level with a sharp drop in summer months followed by a gradual increase heads in winter month. Overall, on annual basis, it is observed that the head is dropping throughout the basin with the rate of drop as high as 2 m/year at some wells.

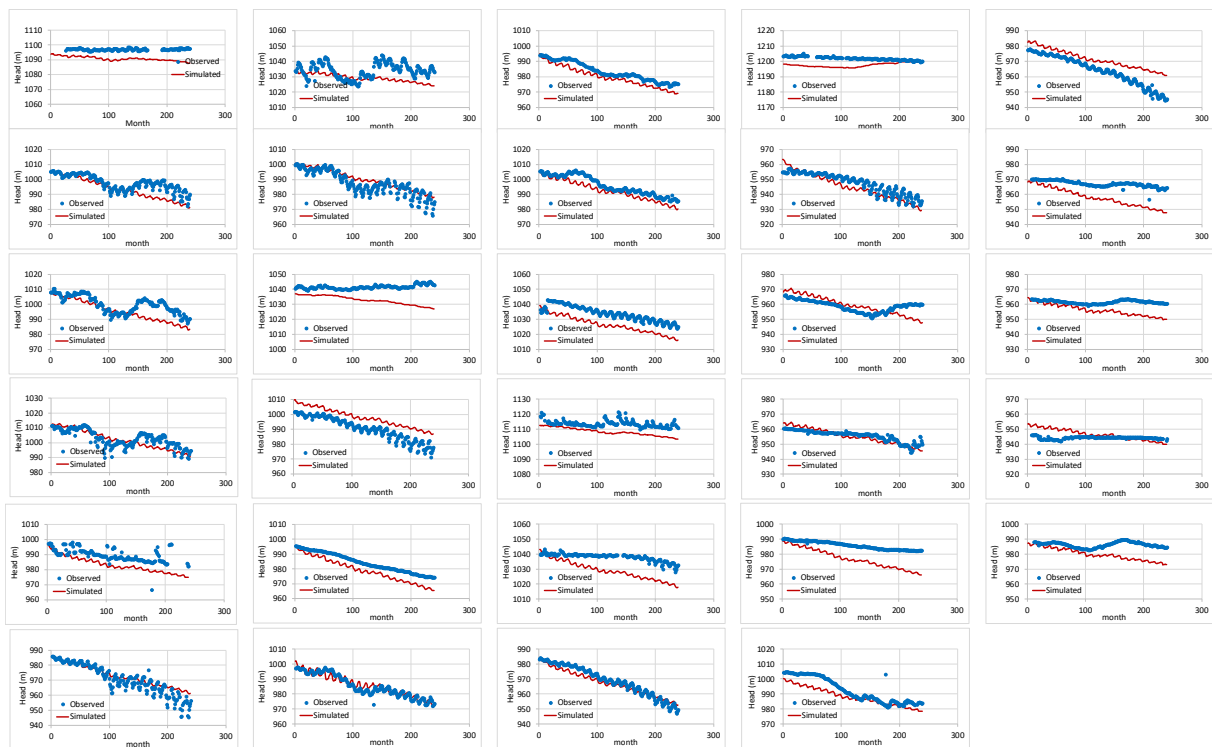


Figure 25. Comparison of the simulated and observed heads

Figure 26 shows the simulated heads at 5-year intervals starting from 2000. The flow is seen to converge towards the north-central part of the basin.

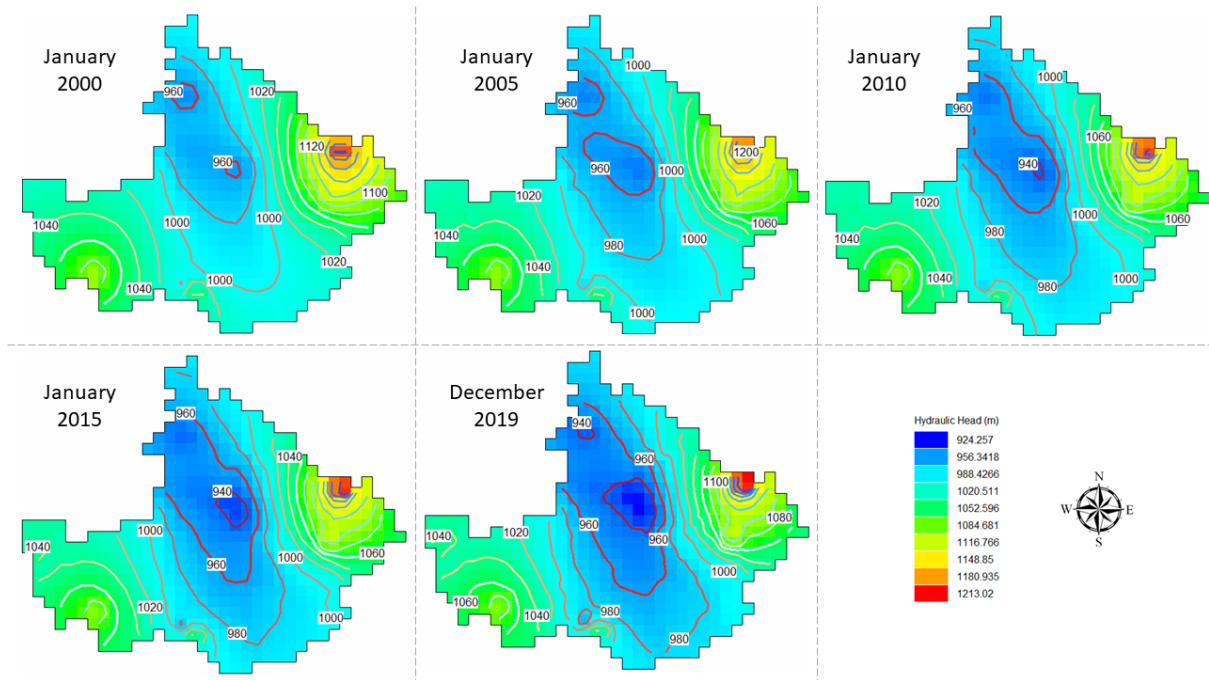


Figure 26. Spatial distribution of the simulated head on January of years 2000, 2005, 2010, 2015 and 2020

### Description of the Surrogate Model

The aim is to build a surrogate model able to provide groundwater levels at 30 control points in the domain (Figure 27). The surrogate model was developed to simulate the observation period (2000-2019). In particular, an Artificial Neural Network (ANN), was trained, validated and tested to replace the numerical forward model.

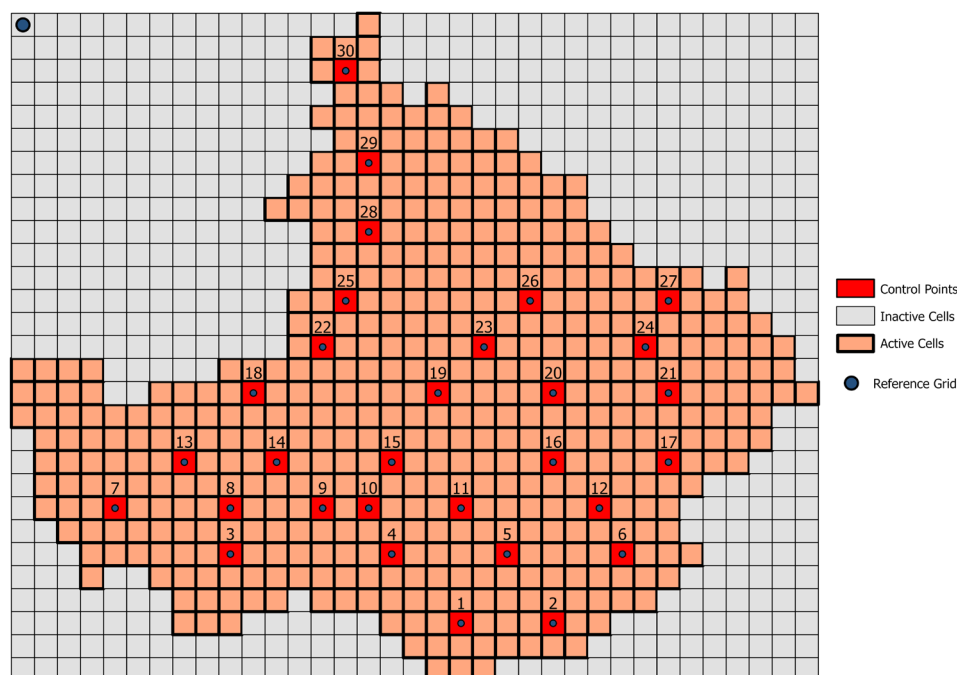


Figure 27. Control Points for Surrogate Model

The first step was to generate the data that will feed the neural network. With this aim, two coefficients were defined: the precipitation coefficient and the crop coefficient. The precipitation and crop coefficients are applied to the historical rainfall and water demand, respectively. The two coefficients, together with the month, was considered as input features, while the 30 control points in the domain were considered as monitoring points of the piezometric head (output features).

A dataset of 100 combinations of precipitation and crop coefficients was generated, using the Latin Hypercube Sampling method, assuming a range of reduction/increase in terms of precipitation equal to  $\pm 40\%$  and water demand equal to  $\pm 25\%$ . Then, the numerical model was run for each combination in the period 2000 and 2019 (20 years), and the values of the piezometric heads, at the 30 control points, were stored with a monthly time discretization (240 months). In summary, for each model run, we obtained a dataset of 240 values of piezometric heads, totaling a dataset with 24,000 data for each control point.

This dataset was used for training (70%), validating (15%) and testing (15%) the neural network (Figure 28).

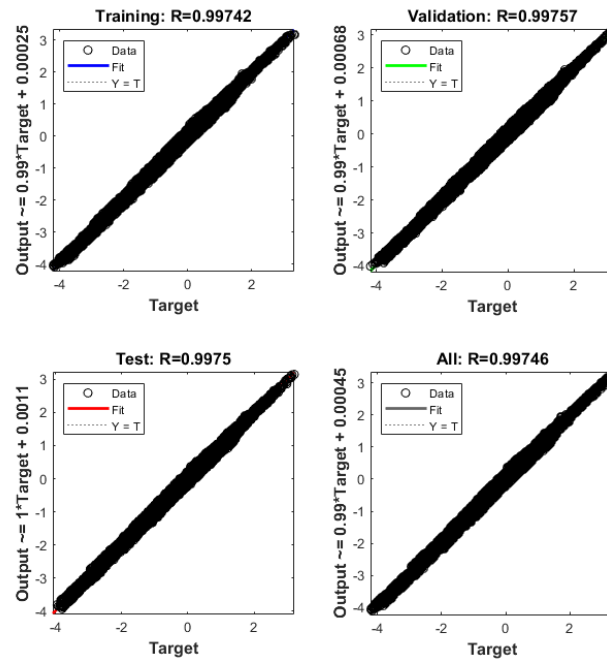


Figure 28. Training, validation and test performances of the ANN for the period 2000-2019

The fully trained network was used to predict groundwater levels at control points. The results are reported in terms of variation of groundwater levels with respect to the starting heads of December 1999. As an example, we presented the results of three different precipitation scenarios: - 20% of the precipitation in the 2000-2019 period (Prec -20%), precipitation in the 2000-2019 period (Prec) and + 20% of the precipitation in the 2000-2019 period (Prec +20%). For each scenario the water demand was considered in the range  $\pm 20\%$  (grey band in Figures 29 – 32).

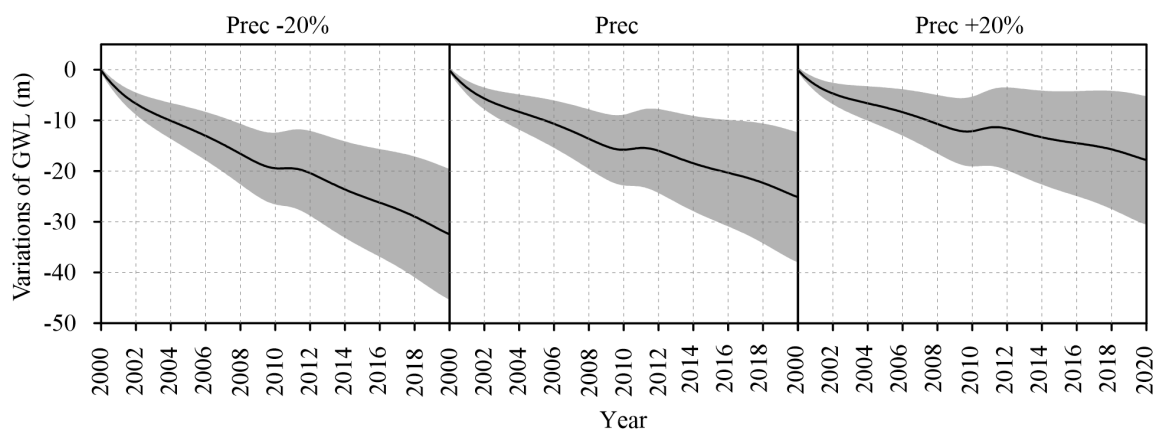


Figure 29. Groundwater level variations vs time at control point 2 for different precipitation scenarios: observed (Prec) and  $\pm 20\%$ . The solid black line depicts the variation of groundwater levels

considering the observed (2000-2009) water demand. The grey band shows the variability of the predicted groundwater levels inside the range  $\pm 20\%$  of the water demand

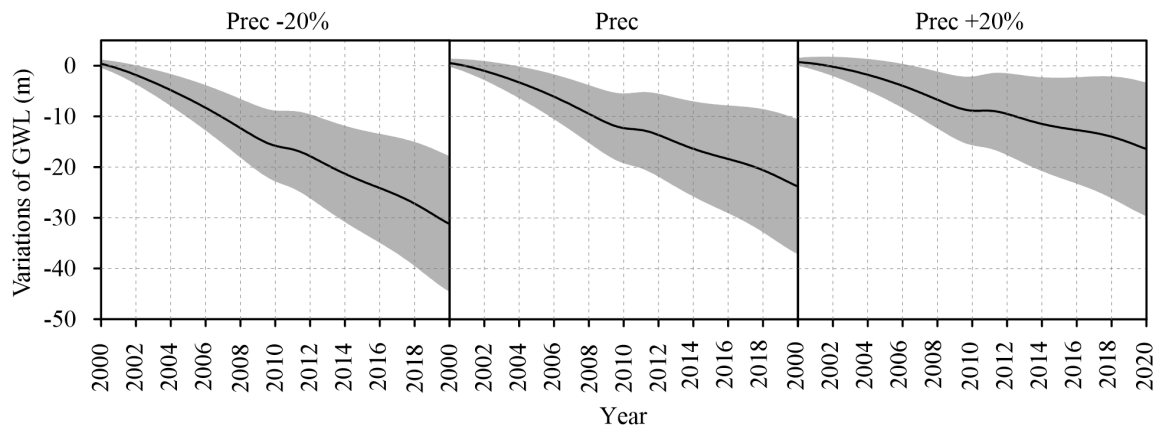


Figure 30. Groundwater level variations vs time at control point 10 for different precipitation scenarios: observed (Prec) and  $\pm 20\%$ . The solid black line depicts the variation of groundwater levels considering the observed (2000-2009) water demand. The grey band shows the variability of the predicted groundwater levels inside the range  $\pm 20\%$  of the water demand

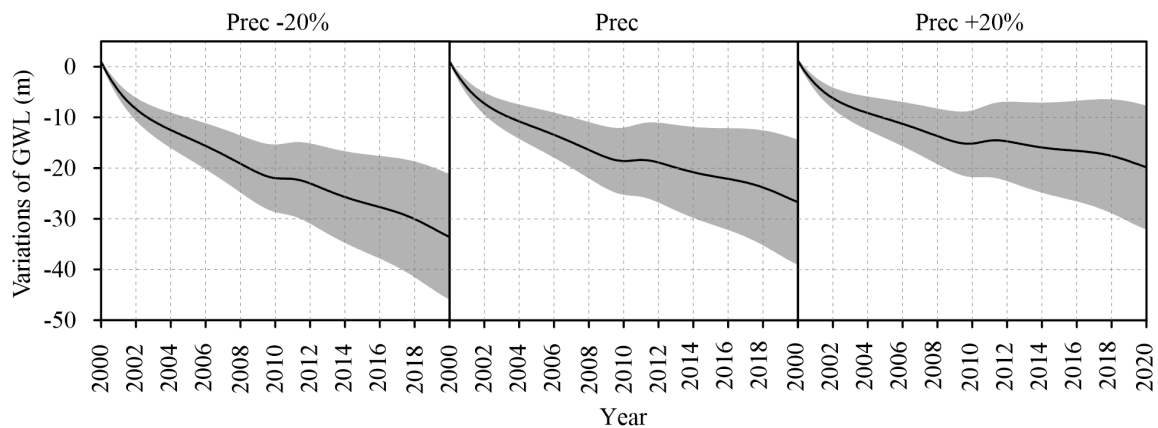


Figure 31. Groundwater level variations vs time at control point 20 for different precipitation scenarios: observed (Prec) and  $\pm 20\%$ . The solid black line depicts the variation of groundwater levels considering the observed (2000-2009) water demand. The grey band shows the variability of the predicted groundwater levels inside the range  $\pm 20\%$  of the water demand

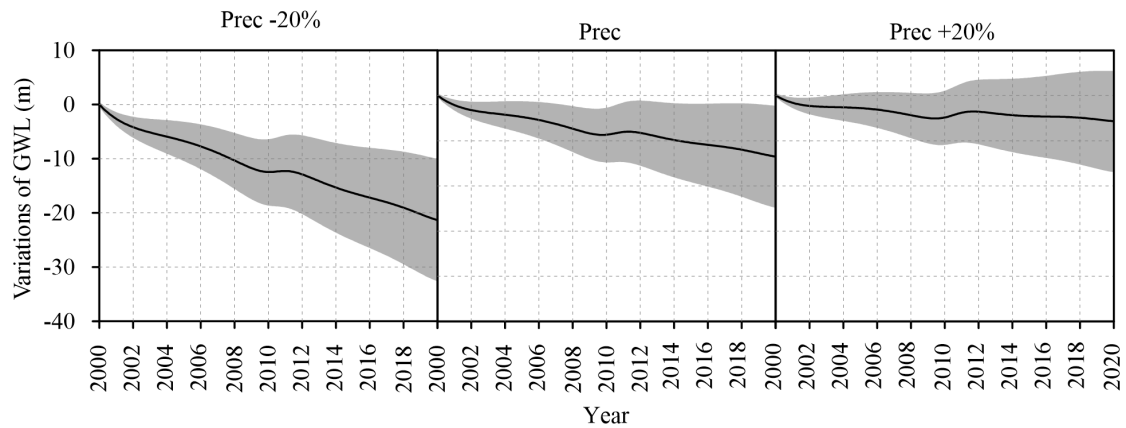


Figure 32. Groundwater level variations vs time at control point 30 for different precipitation scenarios: observed (Prec) and  $\pm 20\%$ . The solid black line depicts the variation of groundwater levels considering the observed (2000-2009) water demand. The grey band shows the variability of the predicted groundwater levels inside the range  $\pm 20\%$  of the water demand

### Future Scenario Analyses

In order to assess the effects of climate change on the investigated aquifer, a surrogate model was developed to replace the numerical model for the future period 2020-2039. The numerical model was calibrated using precipitation data recorded in the years 2000-2019. The same pattern of precipitation was used for the future simulations. Also, in this case, an ANN was considered with the same architecture of the one previously described: 3 input (month, precipitation and crop coefficients) and 30 output features (piezometric heads in the 30 control points). The main difference is represented by the starting heads, that are no longer the piezometric heads recorded in the December 1999, but are the piezometric heads simulated for the December 2019.

The dataset has the same dimension of the previous one (24,000 data for each control point) and was split with the same percentages in training, validation and test sets. Figure 33 depicts the performance of the three phases.

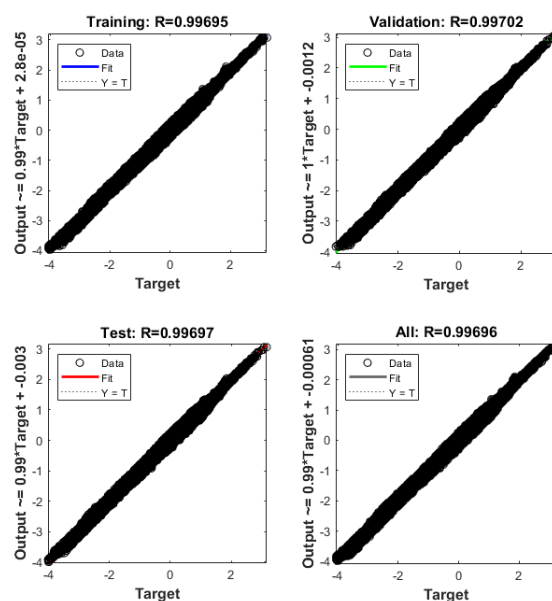


Figure 33. Training, validation and test performances of the ANN for the period 2020-2039

The implemented surrogate model will be used to analyze future scenarios that will be discussed in Deliverable 3.4.

## 2.4. Grombalia (Tunisia)

### Objectives of the Surrogate Model

The objective of the surrogate model developed for the Grombalia aquifer is to provide a quick tool to investigate the impact of future climate scenarios on the groundwater resources.

A complete numerical model is not available for this study area; therefore, a data-driven surrogate model has been developed based on groundwater levels, precipitation and temperature data. Assuming that the hydrological processes will not change over time, the proposed method is a statistical method that allows a fast evaluation of groundwater variations based on precipitation and temperature future scenarios.

### Description of the Data

The involved study area, shown in Figure 34, is the Grombalia shallow aquifer. The available data are precipitation, temperature, groundwater levels, some quality data and exploitation rate. Among the available data, for their abundance of data, we select precipitations recorded



from six gauging stations and temperature from 1 station at a daily scale in the period 1976-2020 (Figure 34 and Table 3). The gaps in the precipitation and temperature time series were filled using the FAO method (Allen et al., 1998). For temperature data, the gaps were filled using the temperature data provided by the WATCH Forcing dataset (WFD; Weedon et al., 2010), which is a twentieth century meteorological forcing dataset that covers from 1958 to 2001 with 0.5 x 0.5 degrees spatial resolution. The WFD temperature records at the four cells closest to the gauging station are analysed and the more correlated with the observed time-series was used to fill the gaps according to the FAO method. The precipitation data have been processed with the Thiessen polygon techniques to obtain precipitation areal averages. Instead, the areal temperature was considered equal to that recorded in the only available station. The climate variables are investigated in terms of Standardized Precipitation Evapotranspiration Indices (SPEIs) computed at different accumulation periods (3, 6, 9, 12, 18, 24 and 36 months). The SPEI is a statistical index useful in detecting the meteorological droughts using monthly differences between precipitation and potential evapotranspiration; (Vicente-Serrano et al. 2010). Figure 35 reports the SPEI computed considering the precipitation and temperature data averaged over the area of interest. SPEI values close to zero indicate conditions close to the average, positive values indicate abundant rains; negative values denote the drought periods. A meteorological drought in the period 2013-2018 is detected for the investigated area.

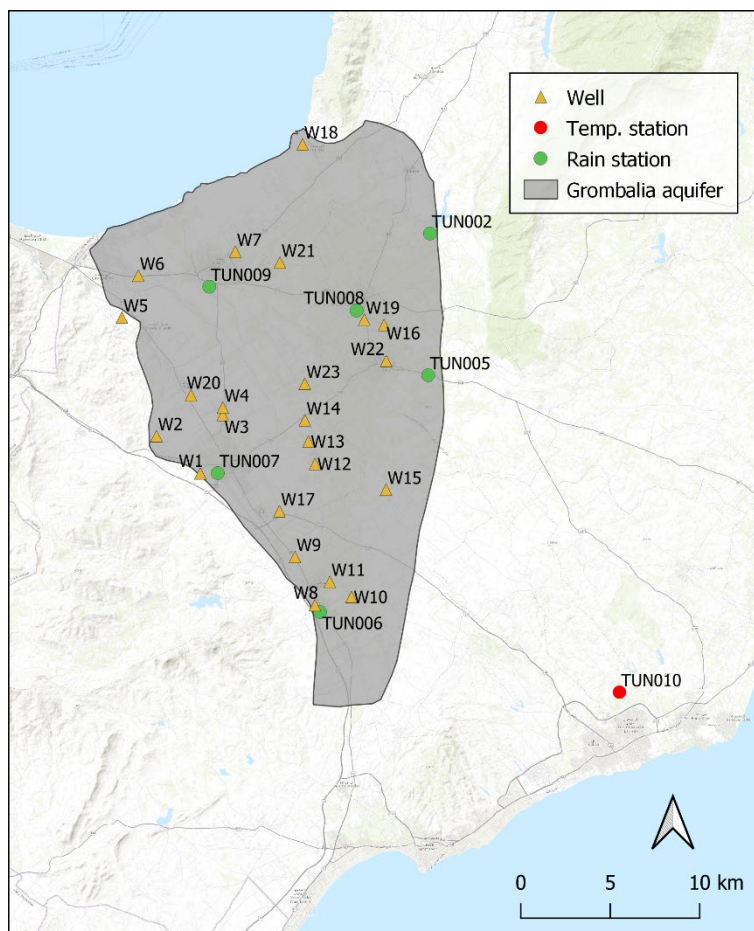


Figure 34. Tunisia: study area and location of the temperature and rain stations and monitoring wells

Table 3. Tunisia: station name and station code of the gauging stations

Station Name	Station code	Rain	Temp
Bezirk Dam	TUN002	X	
Beni Khalled Ferme	TUN005	X	
CTV Bouargoub	TUN006	X	
Grombalia DRE	TUN007	X	
CTV Menzel Bouzelfa	TUN008	X	
CTV Soliman	TUN009	X	
Nabeul	TUN010		X

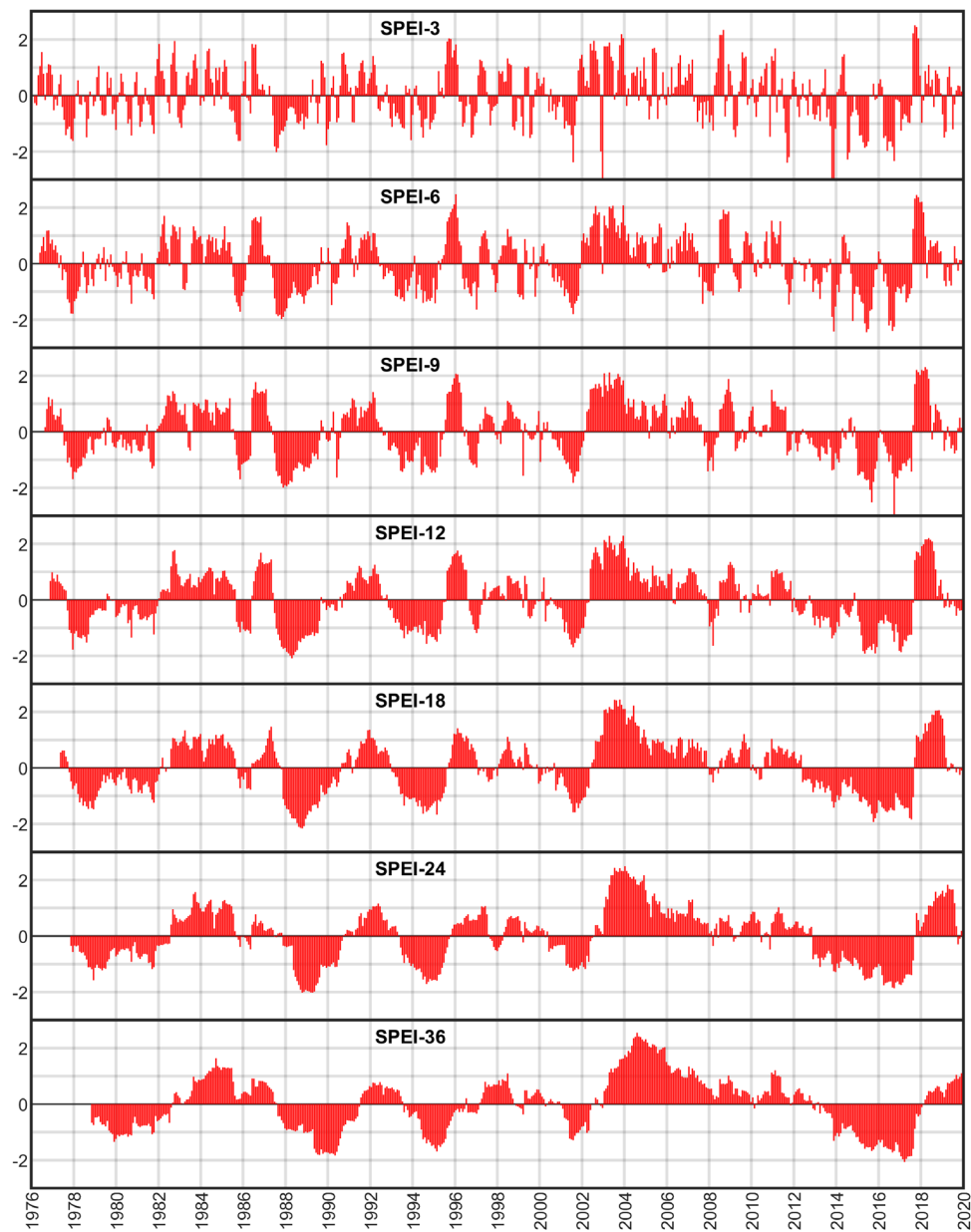


Figure 35. Tunisia: SPEIs for time windows of 3, 6, 9, 12, 18, 24 and 36 months

The groundwater levels were collected from 23 wells in the period 2000-2020 (Figure 34 and Table 4); one or two data per year are available in the period 2000-2020. Figure 36 shows the observed GWLs data with their trend lines. There is not a uniform trend over the considered area; therefore, the analysis was performed at the specific local scale defined by the well locations.

Table 4. Tunisia: name and codes of the monitoring wells

Well Name	Well code	Well Name	Well code
12440	W1	8588	W13
6922	W2	13397	W14
2183	W3	12202	W15
2171	W4	13571	W16
2543	W5	8844	W17
2534	W6	2379	W18
1404	W7	12134	W19
2008	W8	12405	W20
2025	W9	12406	W21
11419	W10	12961	W22
13474	W11	13329	W23
8589	W12		

Regarding the quality data, 3 datasets are available (Table 5). The first, named official points, provide dry residuals and nitrate for 7 monitoring points and 11 sampling campaigns from 2009 to 2019. The second dataset, named InTheMED, provide water quality data for 20 monitoring points for a sampling campaign. The third dataset provides similar information collected for 23 monitoring points and two sampling campaigns in 2000 and 2015. All these datasets have monitoring points at different locations. The last two dataset cannot be used as one or two campaigns are not enough to perform statistical analysis. Figure 37 shows the time series of nitrates provided by the first dataset with their regression lines. There is not a uniform trend over the investigated area. For some wells, the nitrates increase during the 10 considered years, otherwise for some wells a decreasing trend is noticed. The locations of the groundwater monitoring wells and nitrate monitoring wells is not the same; hence, it is not possible to relate nitrate and groundwater levels.

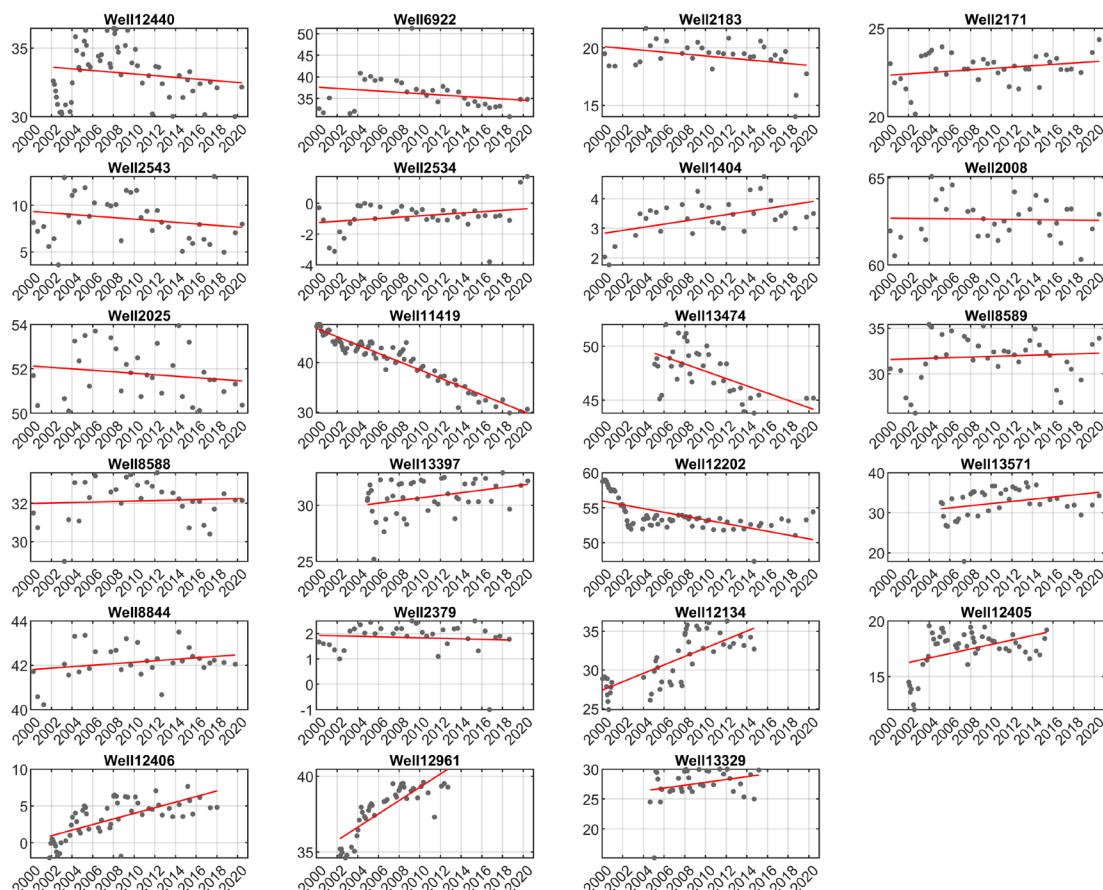


Figure 36. Tunisia: Groundwater levels (m a.s.l.) recorded in the period 2000-2020. The points are the observations and the solid line is the regression line

The exploitation data are available on the whole area collected every five years in the period 1980-2015 (Table 6). However, the dataset presents not enough data for accurate statistical analysis and the location of the exploitation wells is unknown.

For these reasons, the proposed surrogate model considered only the precipitation, temperature and groundwater level data.

Table 5. Tunisia: datasets of quality data.

Dataset	Variable	Monitoring points	Sampling campaigns	Time of record
Official points	Dry residue and nitrate	7	11	2009-2019
InTheMED	Na <sup>+</sup> , NH <sub>4</sub> <sup>+</sup> , K <sup>+</sup> , Ca <sup>2+</sup> , Na <sup>2+</sup> , Mg <sup>2+</sup> , Cl <sup>-</sup> , NO <sup>2-</sup> , NO <sup>3-</sup> , PO <sub>4</sub> <sup>3-</sup> , SO <sub>4</sub> <sup>2-</sup>	20	1	Unknown (recent)

Slama et. al	Salinity, $\text{Na}^+$ , $\text{K}^+$ , $\text{Mg}^{2+}$ , $\text{Ca}^{2+}$ , $\text{SO}_4^{2-}$ , $\text{Cl}^-$ , $\text{HCO}_3^-$	23	2	2000 and 2015
--------------	---	----	---	------------------

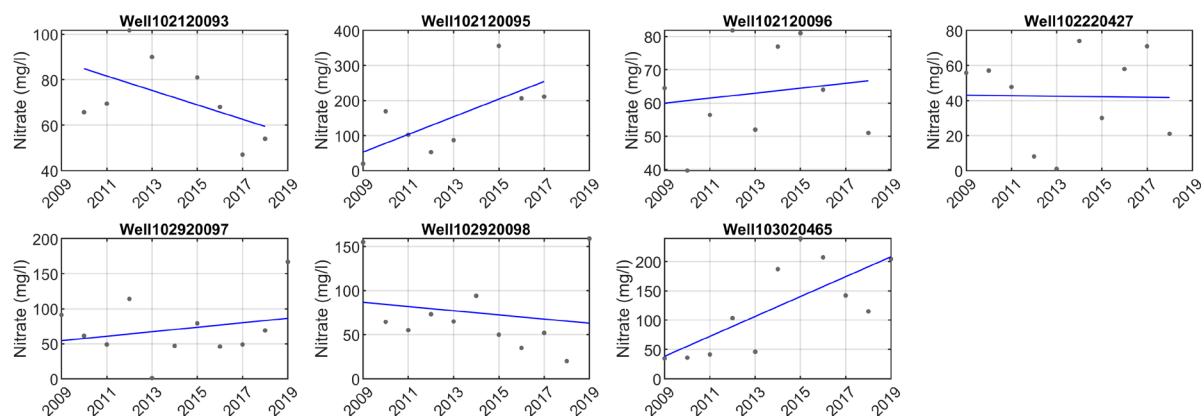


Figure 37. Tunisia: Nitrate recorded in the period 2009-2019. The points are the observations and the solid line is the regression line.

Table 6. Tunisia: exploitation rate data.

Years	Total number of wells	Number of abandoned wells	Exploitation ( $\text{Mm}^3/\text{year}$ )	Estimated renewable resources ( $\text{Mm}^3/\text{year}$ )
1980	5689	53.8	--.--	--.--
1985	5733	60.2	35.7	168.6
1990	8280	89.7	35.5	252.7
1995	8430	90	51	176.5
2000	8408	93	51	182.4
2005	8531	90	51	176.5
2010	8814	104.6	51	205
2015	8814	106	51	207.8

### Description of the Surrogate Model

A simple data-driven surrogate model has been developed to evaluate the impacts of climate change on groundwater levels (Secchi et al., 2021). A linear regression model has been used to describe the relationship between meteorological variables and groundwater levels (GWL).

The first step for the development of the surrogate model is to investigate if the historical rainfall and temperature data, in terms of SPEIs, and groundwater levels collected in monitoring wells are correlated. The meteorological indices and GWL data are defined correlated if the Pearson correlation coefficient is greater than 0.7.

For those wells presenting satisfactory correlation, a linear regression relationship has been computed between GWLs and SPEIs. This linear regression model represents the surrogate model that describes the dependence of groundwater levels on meteorological variables and will be used to evaluate the future groundwater levels based on future SPEI values, estimated by means of an ensemble of regional climate models (RCMs) under different climate scenarios (RCP 4.5 and RCP 8.5).

### **Evaluation of the Performance**

---

The correlation between the GWLs of each well and SPEIs computed at the different time scales have been initially evaluated considering all the available data and then using only GWLs observed in February, March and April. The results are depicted in Figure 38. The Pearson correlation coefficients are very low if computed on all the available data for all wells. On the contrary, correlations increase for some wells if the analysis is computed on the period February-April. This stems for the fact that groundwater resources in these months presents minimal anthropogenic influence due to pumping and irrigation. The wells that do not show correlation for both analyses are likely affected by external factors and they do not respond to the meteorological variables only. Moreover, the results highlight a different sensitivity of the well data to the climate variables; the wells present the highest correlation at different time scale. The groundwater levels respond to the climate variables with different time lag probably due to the distinct characteristics of the aquifer and wells depths.

Therefore, the surrogate model has been developed based on late winter and early spring months data and considering the wells that present at least a Pearson correlation coefficient greater than 0.7, resulting in eight correlated wells. In Figure 39 to Figure 46, the results for all the eight correlated wells are shown; the linear regression models with their confidence interval are depicted.

For future projections (Task 3.4), the regression model calculated considering the SPEI at the time scale with the highest correlation will be used as surrogate model.

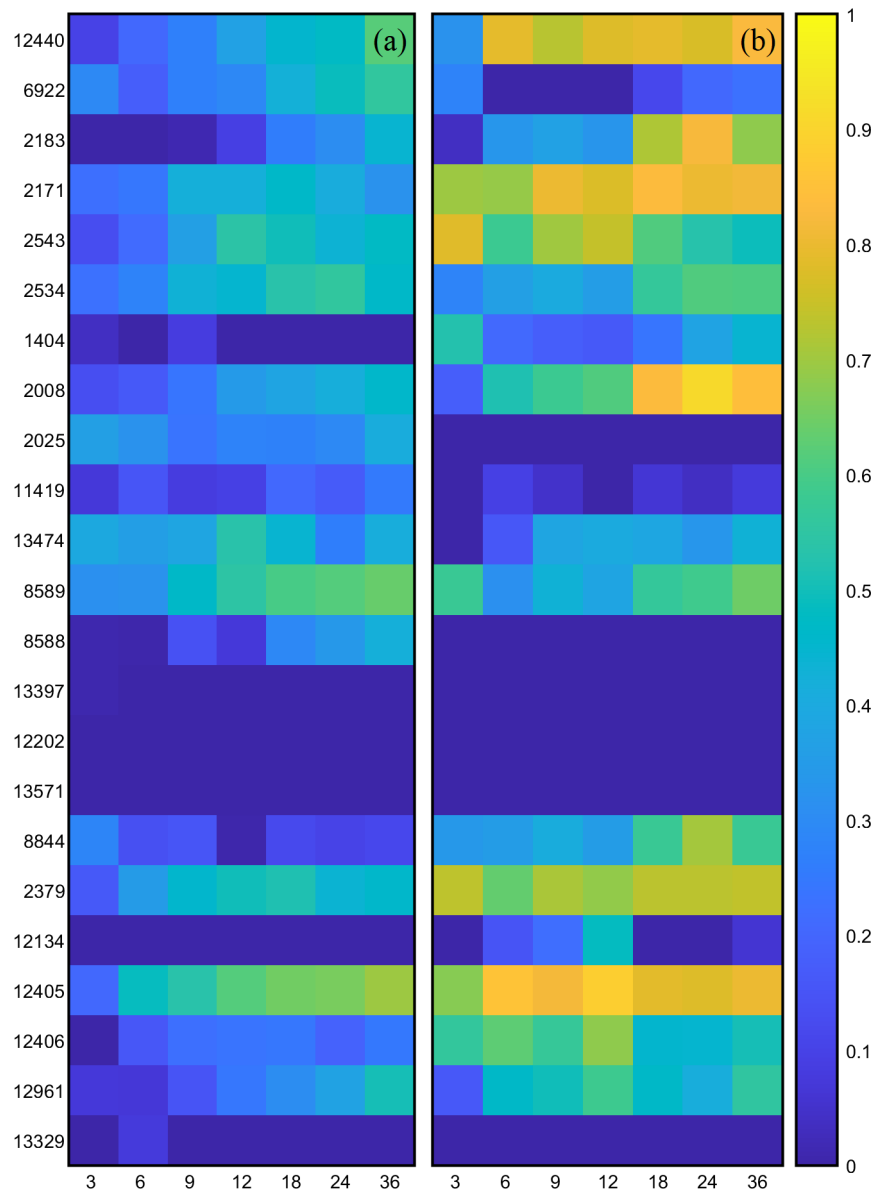


Figure 38. Tunisia: Pearson correlation coefficients between groundwater levels observed at the 23 wells (y-axis) and the and SPEIs at the time scale of 3, 6, 9, 12, 18, 24 and 36 months (x-axes) considering all months (a) and February-April months, respectively



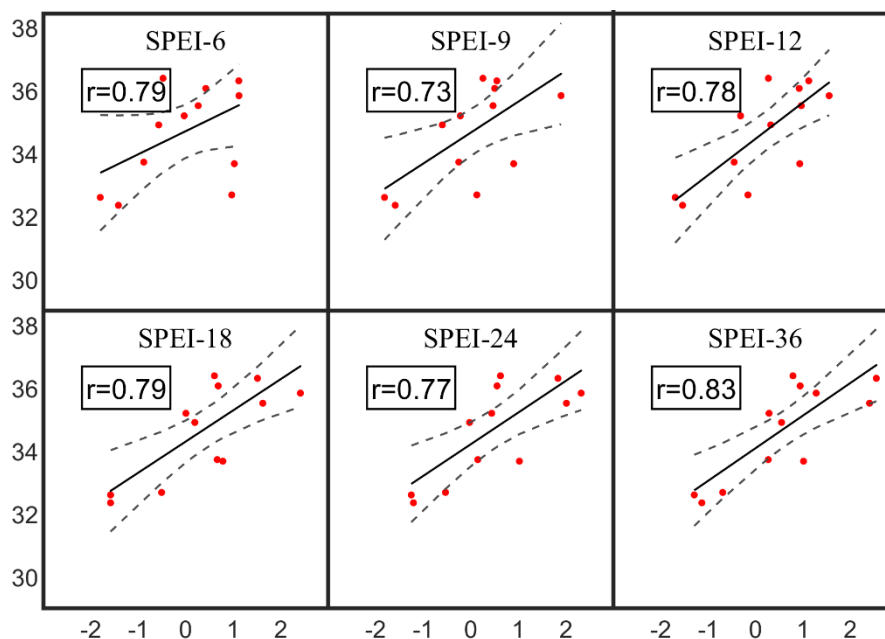


Figure 39. Tunisia: linear regression model for the well 12440. The x-axis shows the SPEI values and the y-axis the groundwater level in m a.s.l. The points are the observed groundwater levels, the solid line is the regression line and the dashed lines are the confidence intervals (95%); the correlation coefficients are reported in the boxes

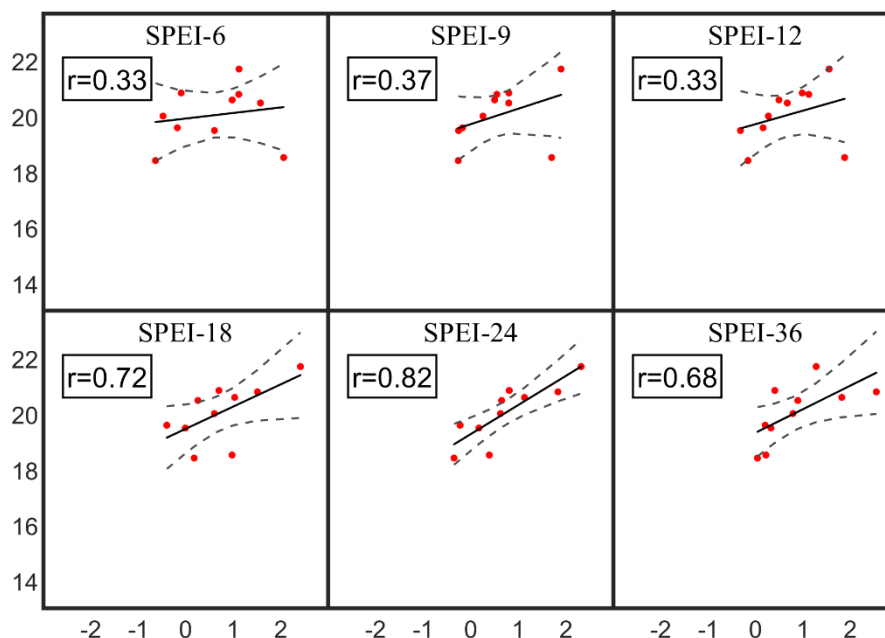


Figure 40. Tunisia: linear regression model for the well 2183. The x-axis shows the SPEI values and the y-axis the groundwater level in m a.s.l. The points are the observed groundwater levels, the solid line is the regression line and the dashed lines are the confidence intervals (95%); the correlation coefficients are reported in the boxes

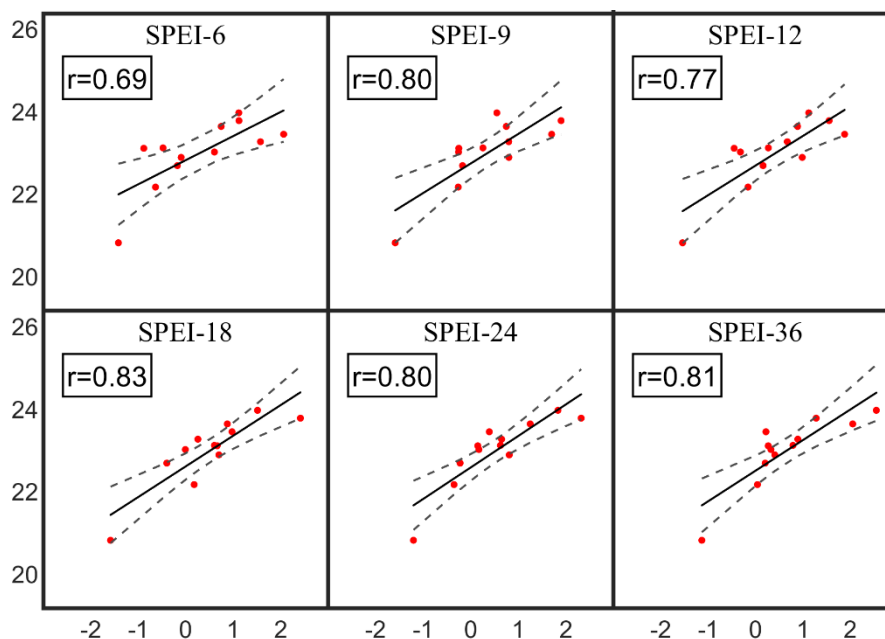


Figure 41. Tunisia: linear regression model for the well 2171. The x-axis shows the SPEI values and the y-axis the groundwater level in m.a.s.l. The points are the observed groundwater levels, the solid line is the regression line and the dashed lines are the confidence intervals (95%); the correlation coefficients are reported in the boxes

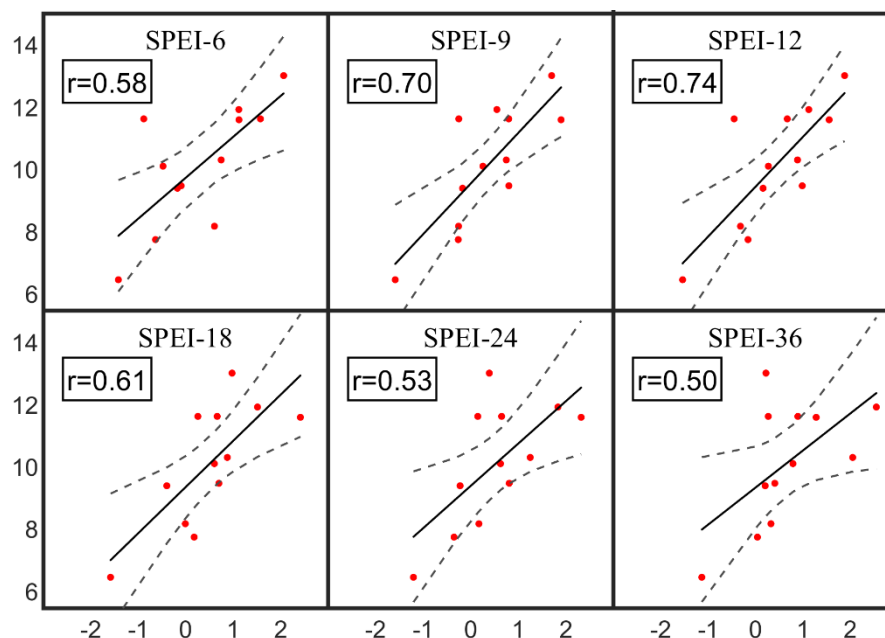


Figure 42. Tunisia: linear regression model for the well 2543. The x-axis shows the SPEI values and the y-axis the groundwater level in m.a.s.l. The points are the observed groundwater levels, the solid line is the regression line and the dashed lines are the confidence intervals (95%); the correlation coefficients are reported in the boxes

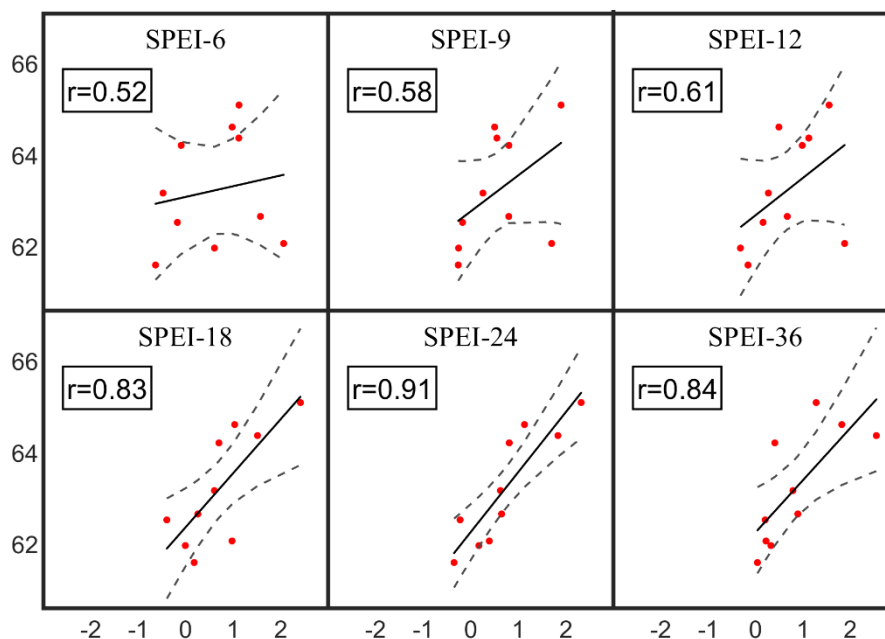


Figure 43. Tunisia: linear regression model for the well 2008. The x-axis shows the SPEI values and the y-axis the groundwater level in m a.s.l. The points are the observed groundwater levels, the solid line is the regression line and the dashed lines are the confidence intervals (95%); the correlation coefficients are reported in the boxes

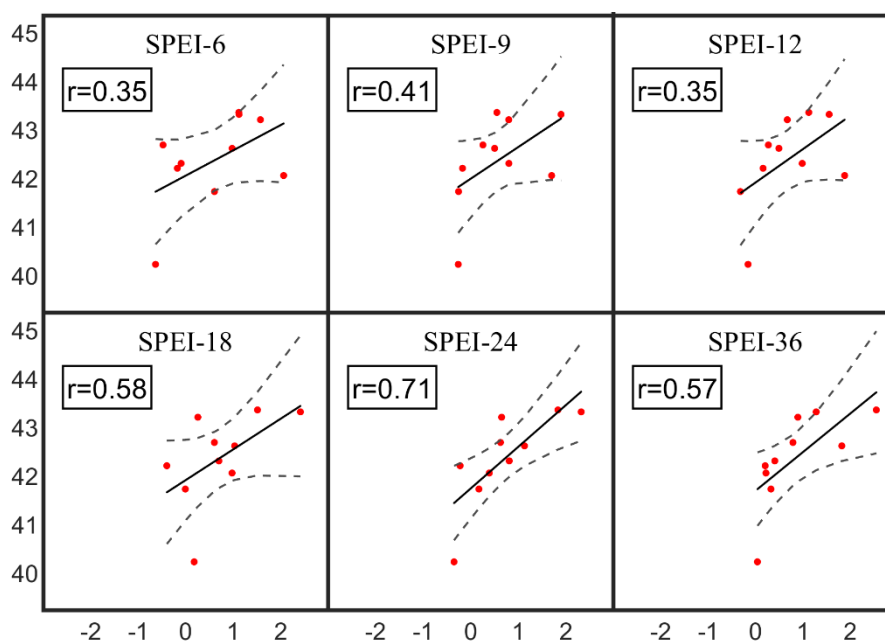


Figure 44. Tunisia: linear regression model for the well 8844. The x-axis shows the SPEI values and the y-axis the groundwater level in m a.s.l. The points are the observed groundwater levels, the solid line is the regression line and the dashed lines are the confidence intervals (95%); the correlation coefficients are reported in the boxes

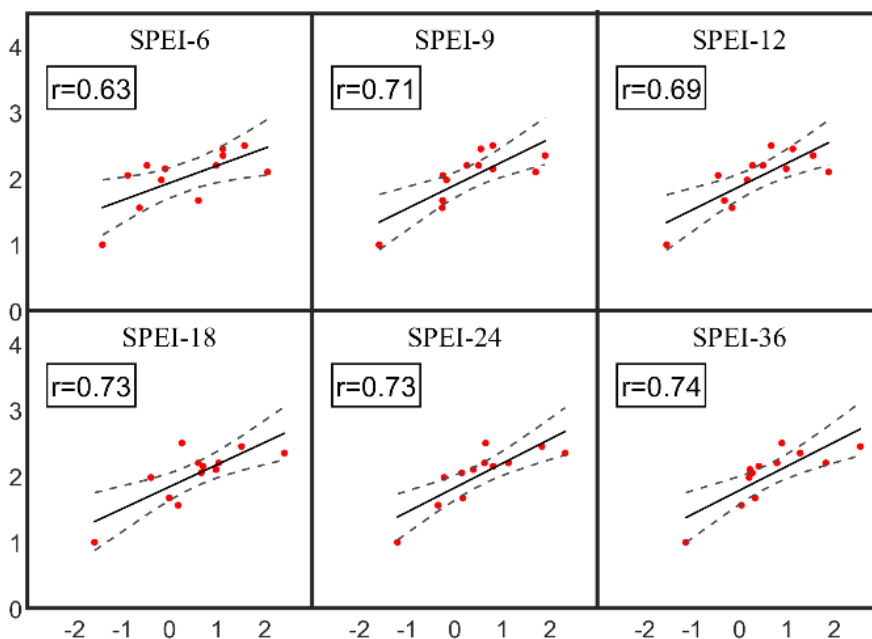


Figure 45. Tunisia: linear regression model for the well 2379. The x-axis shows the SPEI values and the y-axis the groundwater level in m a.s.l. The points are the observed groundwater levels, the solid line is the regression line and the dashed lines are the confidence intervals (95%); the correlation coefficients are reported in the boxes

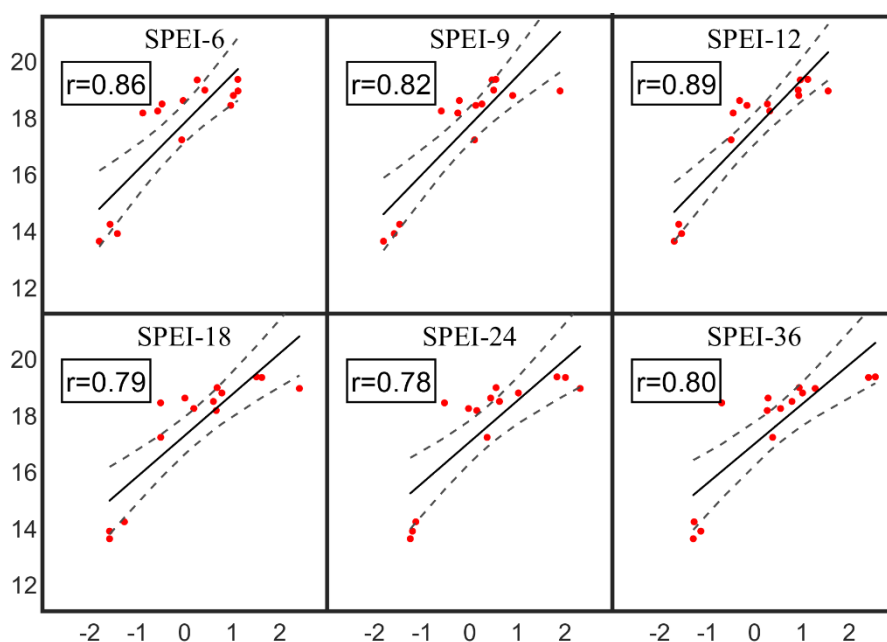


Figure 46. Tunisia: linear regression model for the well 12405. The x-axis shows the SPEI values and the y-axis the groundwater level in m a.s.l. The points are the observed groundwater levels, the solid line is the regression line and the dashed lines are the confidence intervals (95%); the correlation coefficients are reported in the boxes

## 2.5. Castro Verde (Portugal)

### Objectives of the Surrogate Model

The objectives of the surrogate model for Castro Verde (Portugal) are the investigation of potential impacts of climate changes on groundwater availability. Also, for this study area, a complete numerical model is not available and a data-driven surrogate model has been developed based on groundwater levels, precipitation and temperature data. Assuming that the hydrological processes will not change over time, the proposed method is a statistical method that allows a fast evaluation of groundwater variations based on precipitation and temperature future scenarios.

### Description of the Data

Castro Verde case study belongs to the Portuguese South Zone of Guadiana Basin groundwater mass, located in the south part of the Guadiana Hydrographic Basin (Figure 47).

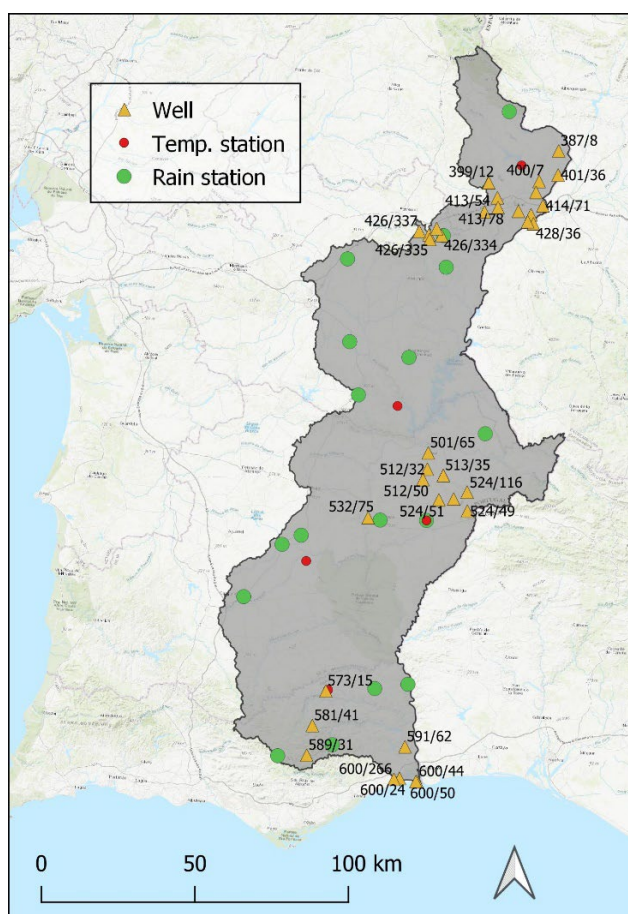


Figure 47. Portugal: study area and location of the selected temperature and rain stations and monitoring wells.

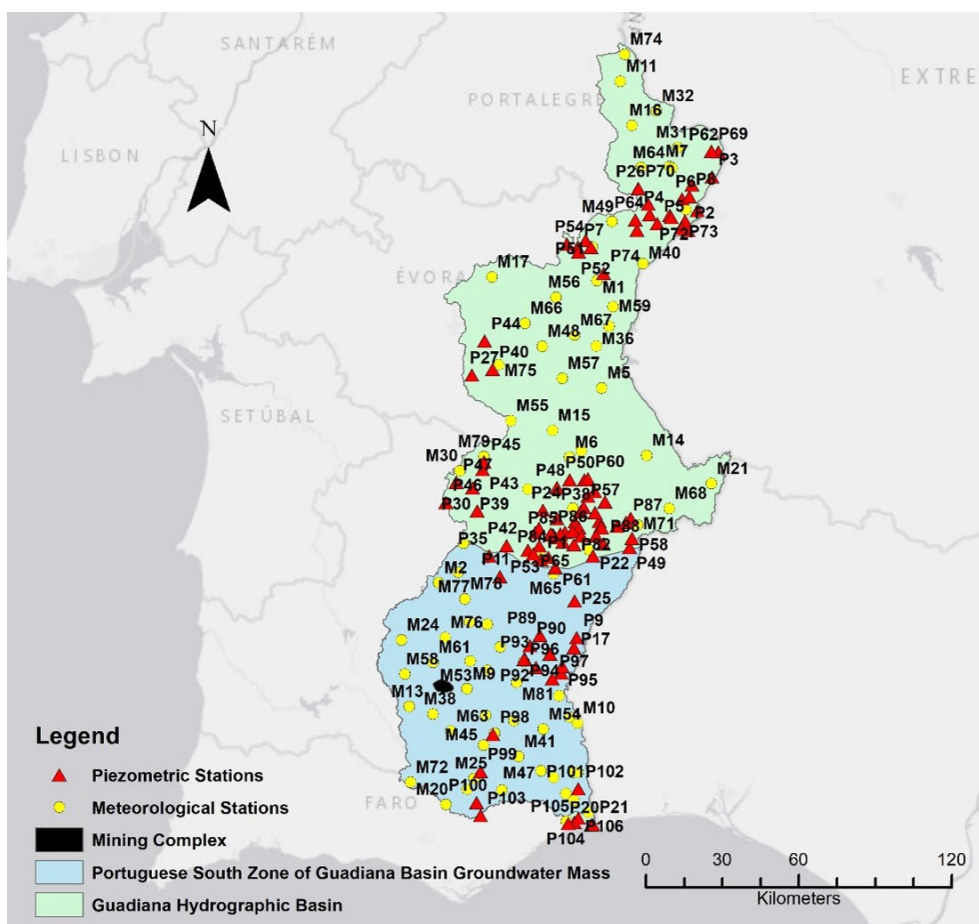


Figure 48. Portugal: study area and locations of the meteorological and piezometric stations (SNIRH)

Both precipitation and temperature data were collected from 81 meteorological stations for an overall period between 1970-2021 (Figure 48 and Table 7). For most of the stations, precipitation data are available on a daily basis, whether throughout the entire period or during a specific range of years. Regarding temperature data, only eleven stations present temperature measurements taken in a daily or monthly frequency, during distinct periods of time. Piezometric data were collected from 106 piezometric stations for an overall period between 1997-2022 (Figure 40 and Table 8). Most of the stations show measurements taken every other month or in a monthly frequency, each one during different periods of time.

Table 7. Portugal: name, code, and reference of the meteorological stations, as well as frequency of measurements, for an overall period between 1970-2021 (SNIRH)

Station Name	Station code	Reference	Precipitation	Temperature
--------------	--------------	-----------	---------------	-------------

			(Frequency of measurements)	(Frequency of measurements)
ALANDROAL	21M/02UG	M1	Daily	None
ALBERNOA	26J/04UG	M2	Daily since 1979	None
ALBUFEIRA DE ODELEITE	30M/05F	M3	Daily from 2004 until 2008	Daily/monthly from 2001 until 2008
ALBUFEIRA DO ALQUEVA	24L/02F	M4	Daily from 2004 until 2007	Daily from 2002 until 2018
ALBUFEIRA DO ALQUEVA (MOURÃO)	22M/05F	M5	Daily from 2004 until 2007	Daily/monthly from 2002 until 2018
ALBUFEIRA DO ALQUEVA ILHA (EDIA)	24L/03C	M6	Daily from 2007 until 2009	None
ALBUFEIRA DO CAIA	19O/02F	M7	Daily from 2002 until 2010	Daily/monthly from 2001 until 2018
ALCARIA (CASTRO MARIM)	30L/04UG	M8	Daily	None
ALCARIA LONGA	28J/01G	M9	Daily	None
ALCOUTIM	29M/01UG	M10	Daily	None
ALEGRETE	18N/02G	M11	Daily since 1980	None
ALGODÔR	27K/01UG	M12	Daily since 1986	None
ALMODÔVAR	28I/01UG	M13	Daily	None
AMARELEJA	24N/01UG	M14	Daily	None
AMIEIRA	24L/01C	M15	Daily	Daily/monthly from 1980 until 2000
Station Name	Station code	Reference	Precipitation (Frequency of measurements)	Temperature (Frequency of measurements)

ARRONCHES	19N/01UG	M16	Daily	None
AZARUJA	21K/01UG	M17	Daily	None
BARRAGEM DO BELICHE	30M/06G	M18	Daily since 2001	None
BARRAGEM DO CAIA	19O/02C	M19	Daily	Daily/monthly from 1970 until 1998 and from 2016 until 2017
BARRANCO DO VELHO	30J/01UG	M20	Daily	None
BARRANCOS	25P/01UG	M21	Daily	None
CAIA (MONTE CALDEIRAS)	20O/02UG	M22	Daily	None
CASTRO MARIM	30M/03UG	M23	Daily	None
CASTRO VERDE	27I/01G	M24	Daily	None
CATRAIA	30J/02G	M25	Daily until 1974	None
CORTE DA VELHA	27K/02UG	M26	Daily	None
CORTE PEQUENA	27J/02U	M27	Daily until 2000	None
CORTES PEREIRAS	29L/02U	M28	Daily from 1996 until 1999	None
CORUJOS	30L/01UG	M29	Daily	None
CUBA	24J/03UG	M30	Daily	None
DEGOLADOS	19O/03UG	M31	Daily since 1980	None
ESPERANÇA	19N/03UG	M32	Daily since 1980	None
FEITEIRA	30J/03G	M33	Daily since 2001	None
FERREIRA CAPELINS	22M/04UG	M34	Daily since 1980	None
FIGUEIRAIS	30M/01G	M35	Daily until 1984	None
Station Name	Station code	Reference	Precipitation (Frequency of measurements)	Temperature (Frequency of measurements)



FORO ESPANHOL	22M/02C	M36	Daily from 1980 until 1999	Daily/monthly from 1980 until 1991
GIÕES	29K/02UG	M37	Daily since 1980	None
GUEDELHAS	29J/05UG	M38	Daily since 1979	None
HERDADE DE VALADA	26M/01C	M39	Daily	Daily/monthly from 1970 until 1989 and from 2000 until 2020
JUROMENHA	21N/01UG	M40	Daily	None
MALFRADES	29K/03UG	M41	Daily since 1980	None
MARTIM LONGO	29K/01C	M42	Daily	Daily/monthly from 1989 until 2008
MERCADOR	30K/01UG	M43	Daily	None
MESQUITA	28L/02UG	M44	Daily since 1980	None
MONTE DA BRINJEIRA	29K/05G	M45	Daily from 2001 until 2017	None
MONTE DA TORRE	25M/03C	M46	Daily from 2001 until 2017	Daily/monthly from 2001 until 2017
MONTE DOS FORTES	29L/03U	M47	Daily from 1983 until 2000	None
MONTOITO	22L/03UG	M48	Daily from 1980 until 2017	None

Station Name	Station code	Reference	Precipitation (Frequency of measurements)	Temperature (Frequency of measurements)
--------------	--------------	-----------	--	--

MURES ASSECA (TERRUGEM)	20M/04G	M49	Daily from 2001 until 2008 and from 2015 until 2017	None
MÉRTOLA	28L/01UG	M50	Daily	None
PEDROGÃO DO ALENTEJO	25L/01UG	M51	Daily	None
PENEDOS	29K/04UG	M52	Daily since 1980	None
PENILHOS	28J/02UG	M53	Daily from 2001 until 2008 and from 2014 until 2017	None
PEREIRO	29L/01UG	M54	Daily	None
PORTEL	24K/01UG	M55	Daily	None
REDONDO	22L/01U	M56	Daily until 1999	None
REGUENGOS	23L/01G	M57	Daily	None
ROSÁRIO (ALMODÔVAR)	28I/02U	M58	Daily from 1983 until 2000	None
ROSÁRIO (CAPELINS)	22M/03UG	M59	Daily from 1980 until 2017	None
SALVADA	26K/01UG	M60	Daily	None
SANTA BARBARA DE PADRÕES	28J/03UG	M61	Daily from 1979 until 2017	None
SANTA CLARA DO LOUREDO	26J/03UG	M62	Daily from 1979 until 2017	None
SANTA CRUZ	29J/03UG	M63	Daily from 1980 until 2017	None
SANTA EULÁLIA	19N/02U	M64	Daily until 2000	None
Station Name	Station code	Reference	Precipitation (Frequency of measurements)	Temperature (Frequency of measurements)
SANTA IRIA	26L/02UG	M65	Daily from 1980 until 2017	None

SANTA SUSANA	22L/02UG	M66	Daily	None
SANTIAGO MAIOR	22M/01UG	M67	Daily	None
SANTO ALEIXO DA RESTAURAÇÃO	25O/01UG	M68	Daily	None
SAPAL DE ODELEITE (Ex. FONTE DO PENEDO)	29M/02UG	M69	Daily from 1992 until 1999	None
SERPA	26L/01UG	M70	Daily	None
SOBRAL DA ADIÇA	25N/01UG	M71	Daily from 1980 until 2017	None
SOBREIRA	30I/02UG	M72	Daily until 2017	None
SÃO JOÃO DOS CALDEIREIROS	28K/01UG	M73	Daily from 1983 until 2010	None
SÃO JULIÃO	18N/01UG	M74	Daily since 1980	None
SÃO MANÇOS	23K/01UG	M75	Daily	None
SÃO MARCOS DA ATABOEIRA	27J/01UG	M76	Daily from 1972 until 2010	None
TRINDADE	26J/01UG	M77	Daily	None
VALE DE CAMELOS	27J/03C	M78	Daily from 1989 until 2016	Daily/monthly from 1989 until 2016
VIDIGUEIRA	24K/02UG	M79	Daily until 2016	None
VILA VIÇOSA	21M/01UG	M80	Daily	None
ÁLAMO	28K/02UG	M81	Daily since 1980	None

Table 8. Portugal: Name, code, and reference of the piezometric stations, as well as frequency of measurements taken for an overall period between 1997-2022(SNIRH)

Station Name	Station code	Reference	Frequency of measurements
AC 8	532/136	P1	Monthly/every 2 months from 2000 until 2002

AC1 - Monte da Vinha	428/36	P2	Monthly/every 2 months from 2004 until 2022
AC2 - Roças de Baixo	401/36	P3	Monthly/every 2 months from 2004 until 2022
Algaravenha	413/78	P4	Monthly/every 2 months from 1999 until 2007
Amada	428/17	P5	Monthly/every 2 months from 1998 until 2006
Atalaia	414/68	P6	Monthly/every 2 months from 1998 until 2004
BARRO BRANCO	426/302	P7	Monthly/every 2 months from 1997 until 2007
Barrancas	414/67	P8	Monthly/every 2 months from 1998 until 2022
CP 1	551/27	P9	Monthly/every 2 months from 2000 until 2004
CP 1/93	522/200	P10	Monthly/every 2 months from 2000 until 2004
CP2	532/211	P11	Monthly since 2021
Caia	414/71	P12	Monthly/every 2 months from 1998 until 2022
Campo	414/70	P13	Monthly/every 2 months from 1998 until 2007
Carrascal	426/348	P14	Monthly/every 2 months from 1997 until 2022
Ccanas	512/32	P15	Monthly/every 2 months from 2000 until 2022
Station Name	Station code	Reference	Frequency of measurements
Elvas	414/45	P16	Monthly/every 2 months from 1997 until 2007
FURO 2	559/21	P17	Monthly/every 2 months from 2000 until 2004

FURO DOS POMARES	512/212	P18	Monthly/every 2 months from 2016 until 2017
GARGALÃO	524/116	P19	Monthly/every 2 months from 2011 until 2022
JK 10	600/50	P20	Monthly/every 2 months from 1997 until 2022
JK 4 S09	600/44	P21	Monthly/every 2 months from 1997 until 2022
LF 4	533/51	P22	Monthly/every 2 months from 2000 until 2004
Monte Soares	427/24	P23	Monthly/every 2 months from 2003 until 2006
PFT 1	511/71	P24	Monthly/every 2 months from 2000 until 2003
PFT 1	542/19	P25	Monthly/every 2 months from 2000 until 2004
Pena Clara	399/12	P26	Monthly/every 2 months from 1998 until 2007
Poço Alamo-Cabida	471/81	P27	Monthly/every 2 months from 2016 until 2017
Poço Barranco da Aldeia dos Testudos	522/253	P28	Monthly/every 2 months from 2016 until 2017
Poço Horta dos Coentros	522/255	P29	Monthly/every 2 months from 2016 until 2017
Poço Monte das Caldeiras	510/65	P30	Monthly/every 2 months from 2016 until 2017
Station Name	Station code	Reference	Frequency of measurements
Poço de Pias	523/70	P31	Monthly/every 2 months from 2016 until 2017
Poço em Calijos	533/74	P32	Monthly/every 2 months from 2016 until 2017

Poço na Herdade Vale do Carvão	501/311	P33	Monthly/every 2 months from 2016 until 2017
Poço na Herdade de Belmeque	524/114	P34	Monthly/every 2 months from 2016 until 2017
Poço na Horta da Genoveva	531/46	P35	Few measurements between 2016 and 2017
Poço no Aguiheiro	512/215	P36	Monthly/every 2 months from 2016 until 2017
Poço no Cangueiro	523/68	P37	Monthly/every 2 months from 2016 until 2017
Poço no Monte Branco	512/211	P38	Monthly/every 2 months from 2016 until 2017
Poço no Monte da Morena	510/68	P39	Monthly/every 2 months from 2016 until 2017
Poço no Monte das Faias	471/82	P40	Monthly/every 2 months from 2016 until 2017
Poço no Monte das Palmeiras	523/72	P41	Monthly/every 2 months from 2016 until 2017
Poço no Monte de Magalhães	522/254	P42	Monthly/every 2 months from 2016 until 2017
Poço no Monte do Lisboa	499/204	P43	Monthly/every 2 months from 2016 until 2017
Poço no Monte do Louseiro	460/255	P44	Monthly/every 2 months from 2016 until 2017
Poço no Monte do Moinho Branco	499/203	P45	Monthly/every 2 months from 2016 until 2017

Station Name	Station code	Reference	Frequency of measurements
Poço no Monte do Outeiro	510/66	P46	Monthly/every 2 months from 2016 until 2017
Poço no Monte dos Atafuis	499/202	P47	Monthly/every 2 months from 2016 until 2017

Poço nos Calços	512/210	P48	Monthly/every 2 months from 2016 until 2017
RF 1	524/85	P49	Monthly/every 2 months from 2000 until 2004
SD3 Bicas1	501/63	P50	Monthly/every 2 months from 2001 until 2002
SDH1-VILA VIÇOSA	426/334	P51	Monthly/every 2 months from 1997 until 2022
SDH2 - RIO DE MOÍNHOS	426/335	P52	Monthly/every 2 months from 1997 until 2022
SDH3 - Monte da Lobata	532/75	P53	Monthly/every 2 months from 2000 until 2022
SDH4 - NORA	426/337	P54	Monthly/every 2 months from 1997 until 2022
SH LAMEIRA 1	513/34	P55	Monthly/every 2 months from 2000 until 2022
SH LAMEIRA 2	513/35	P56	Monthly/every 2 months from 2011 until 2022
SH MONTE BRANCO 1	512/50	P57	Monthly/every 2 months from 2000 until 2022
SH PALHAIS 2	524/49	P58	Monthly/every 2 months from 2000 until 2022
SH ROSA DA LAVADA 1	524/50	P59	Monthly/every 2 months from 2000 until 2022
SH SANTO ANTÓNIO 2	501/65	P60	Monthly/every 2 months from 2000 until 2022

Station Name	Station code	Reference	Frequency of measurements
SI1	533/43	P61	Monthly/every 2 months from 2000 until 2003

Salvador	387/4	P62	Monthly/every 2 months from 1999 until 2007
Sto António	413/123	P63	Monthly/every 2 months from 1997 until 2007
TCN1 - Vila Boim	413/54	P64	Monthly/every 2 months from 1997 until 2007
TS 1	532/153	P65	Monthly/every 2 months from 2000 until 2004
TS 3	524/82	P66	Monthly/every 2 months from 2000 until 2004
TS 4	524/83	P67	Monthly/every 2 months from 2000 until 2002
Vale Vargo	524/51	P68	Monthly/every 2 months from 1997 until 2022
-	387/8	P69	Monthly/every 2 months from 2011 until 2022
-	399/6	P70	Monthly/every 2 months from 2010 until 2022
-	400/7	P71	Monthly/every 2 months from 1999 until 2020
-	414/116	P72	Monthly/every 2 months from 2008 until 2022
-	428/37	P73	Monthly/every 2 months from 2010 until 2022
-	441/10	P74	Monthly/every 2 months from 1997 until 1999

Station Name	Station code	Reference	Frequency of measurements
-	523/29	P75	Monthly/every 2 months from 2000 until 2002



-	523/30	P76	Monthly/every 2 months from 2000 until 2004
-	523/31	P77	Monthly/every 2 months from 2000 until 2002
-	523/32	P78	Monthly/every 2 months from 2000 until 2003
-	523/33	P79	Monthly/every 2 months from 2000 until 2004
-	523/36	P80	Monthly/every 2 months from 2000 until 2004
-	523/38	P81	Monthly/every 2 months from 2000 until 2004
-	523/40	P82	Monthly/every 2 months from 2000 until 2004
-	523/41	P83	Monthly/every 2 months from 2000 until 2002
-	523/42	P84	Monthly/every 2 months from 2000 until 2002
-	523/43	P85	Monthly/every 2 months from 2000 until 2002
-	523/44	P86	Monthly/every 2 months from 2000 until 2002
-	524/40	P87	Monthly/every 2 months from 2006 until 2007
-	524/60	P88	Monthly/every 2 months from 2000 until 2001

Station Name	Station code	Reference	Frequency of measurements
-	550/28	P89	Monthly/every 2 months from 2000 until 2002

-	558/11	P90	Monthly/every 2 months from 2000 until 2002
-	558/49	P91	Monthly/every 2 months from 2000 until 2004
-	558/52	P92	Monthly/every 2 months from 2000 until 2002
-	558/53	P93	Monthly/every 2 months from 2000 until 2004
-	559/1	P94	Monthly/every 2 months from 2000 until 2004
-	559/17	P95	Monthly/every 2 months from 2000 until 2002
-	559/25	P96	Monthly/every 2 months from 2000 until 2002
-	567/11	P97	Monthly/every 2 months from 2000 until 2002
-	573/15	P98	Monthly/every 2 months from 1999 until 2022
-	581/41	P99	Monthly/every 2 months from 1999 until 2022
-	589/31	P100	Monthly/every 2 months from 1999 until 2015
-	591/62	P101	Monthly/every 2 months from 1999 until 2012
-	591/94	P102	Monthly/every 2 months from 2012 until 2022

Station Name	Station code	Reference	Frequency of measurements
-	598/143	P103	Single measurement in 1996

-	600/24	P104	Monthly/every 2 months from 2009 until 2022
-	600/266	P105	Monthly/every 2 months from 2015 until 2022
-	600/28	P106	Monthly/every 2 months from 2009 until 2015

Among the available monitoring well series, 37 wells were considered for their data abundance (Figure 41). We have selected wells that have at least 50 monthly records; Figure 49 shows the observed data with their trend lines. There is not a uniform trend over the considered area; therefore, the analysis was performed at the specific local scale defined by the well locations.

The precipitation and temperature data used in this analysis involve 17 rain gauges and 5 temperature stations selected for their data abundance in the period 1997-2021 (Figure 47). The gaps in the precipitation and temperature time series were filled using the FAO method (Allen et al., 1998). The data have been processed with the Thiessen polygon techniques to obtain precipitation and temperature areal averages.

The climate variables are investigated in terms of Standardized Precipitation Evapotranspiration Indices (SPEIs) computed at different accumulation periods (1, 3, 6, 9, 12, 18, 24 and 36 months). The SPEI is a statistical index useful in detecting the meteorological droughts using monthly differences between precipitation and potential evapotranspiration; (Vicente-Serrano et al. 2010). Figure 50 reports the SPEI computed considering the precipitation and temperature data averaged over the area of interest. SPEI values close to zero indicate conditions close to the average, positive values indicate abundant rains; negative values denote the drought periods. A meteorological drought period that starts in 2009 is detected for the last decade.

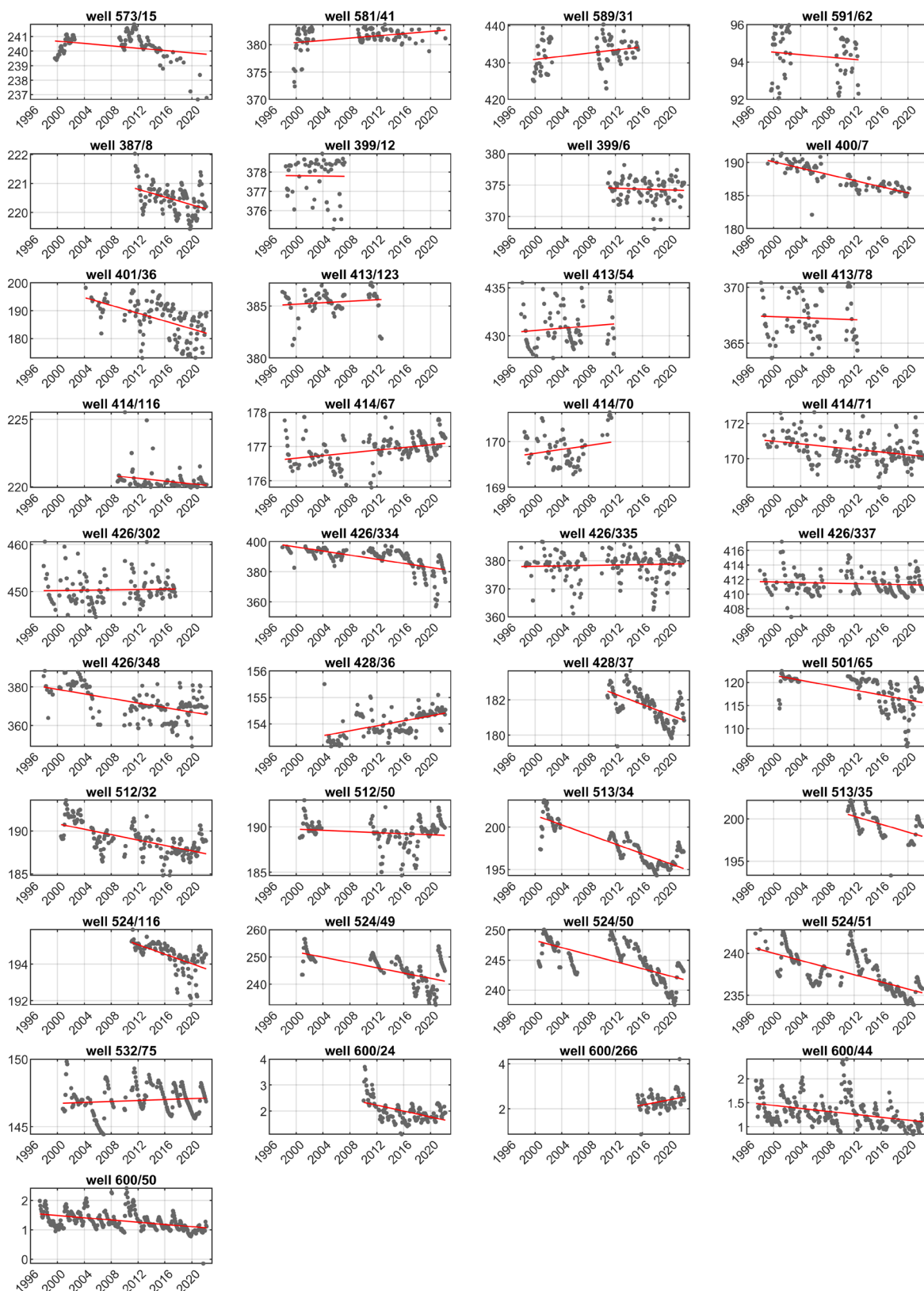


Figure 49. Portugal: groundwater levels (m a.s.l.) recorded in the period 1997-2021. The points are the observations and the solid line is the regression line

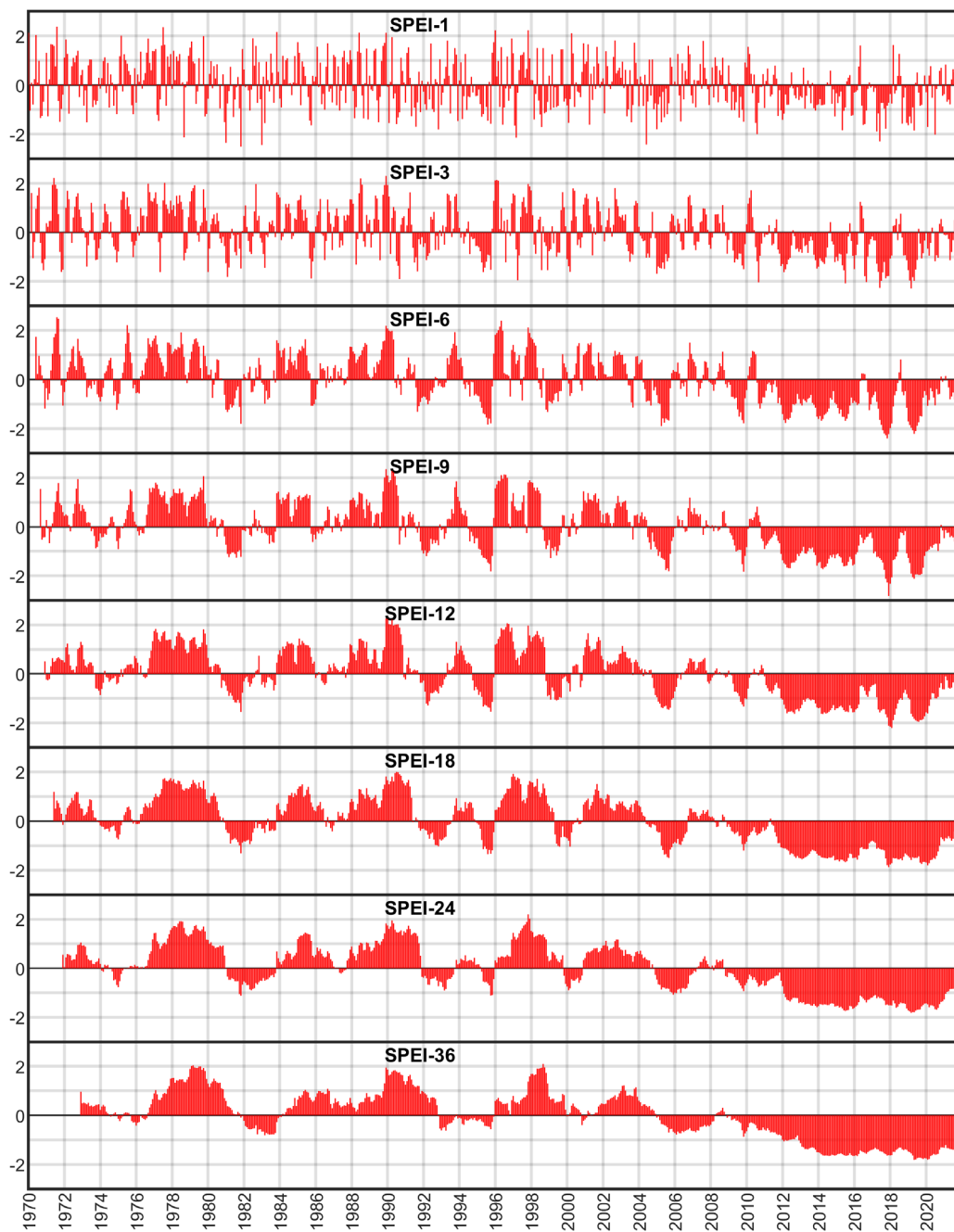


Figure 50. Portugal: SPEIs for time windows of 1, 3, 6, 9, 12, 18, 24 and 36 months

### Description of the Surrogate Model

A simple data-driven surrogate model has been developed to evaluate the impacts of climate change on groundwater levels (Secci et al., 2021). A linear regression model has been used to describe the relationship between meteorological variables and groundwater levels (GWL). The first step for the development of the surrogate model is to investigate if the historical

rainfall and temperature data, expressed in terms of SPEIs, and groundwater levels collected in monitoring wells are correlated. The meteorological indices and GWL data are defined correlated if the Pearson correlation coefficient is greater than 0.7.

For those wells presenting satisfactory correlation, a linear regression relationship has been computed between GWLs and SPEIs. This linear regression model represents the surrogate model that describes the dependence of groundwater levels on meteorological variables and will be used to evaluate the future groundwater levels based on future SPEI values, estimated by means of an ensemble of regional climate models (RCMs) under different climate scenarios (RCP 4.5 and RCP 8.5).

### Evaluation of the Performance

---

The correlation between the GWLs of each well and SPEIs computed at the different time scales have been initially evaluated considering all the available data and then using only GWLs observed in February, March and April. The results are depicted in Figure 3136. For wells that present less than 20 data in the considered period, the correlation coefficients were set equal to zero. The correlations increase for some wells if the analysis is computed on the period February-April. This stems for the fact that groundwater resources in these months presents minimal anthropogenic influence due to pumping and irrigation. The wells that do not show correlation for both analyses are likely affected by external factors and they do not respond to the meteorological variables only. The GWL data are correlated with SPEI at different time scale probably due to the distinct characteristics of the aquifer and wells depths. Most of the wells present the highest correlation with the largest time scale (36 months) denoting that groundwater levels respond to the climate variables with a large time lag. This is due to the presence of many dams and artificial lakes among which Alqueva Dam that creates the largest artificial lake in Europe. The reservoirs could have multi-year regulation that can mask the dependence from the natural hydrological cycles.

The surrogate model has been developed based on late winter and early spring months data and considering the wells that present at least a Pearson correlation coefficient greater then 0.7, resulting in six correlated wells. From Figure 52 to Figure 57, the results for the six correlated wells are shown; the linear regression models with their confidence interval are depicted.

For future projections (Task 3.4), the regression model calculated considering the SPEI at the time scale with the highest correlation will be used as surrogate model.

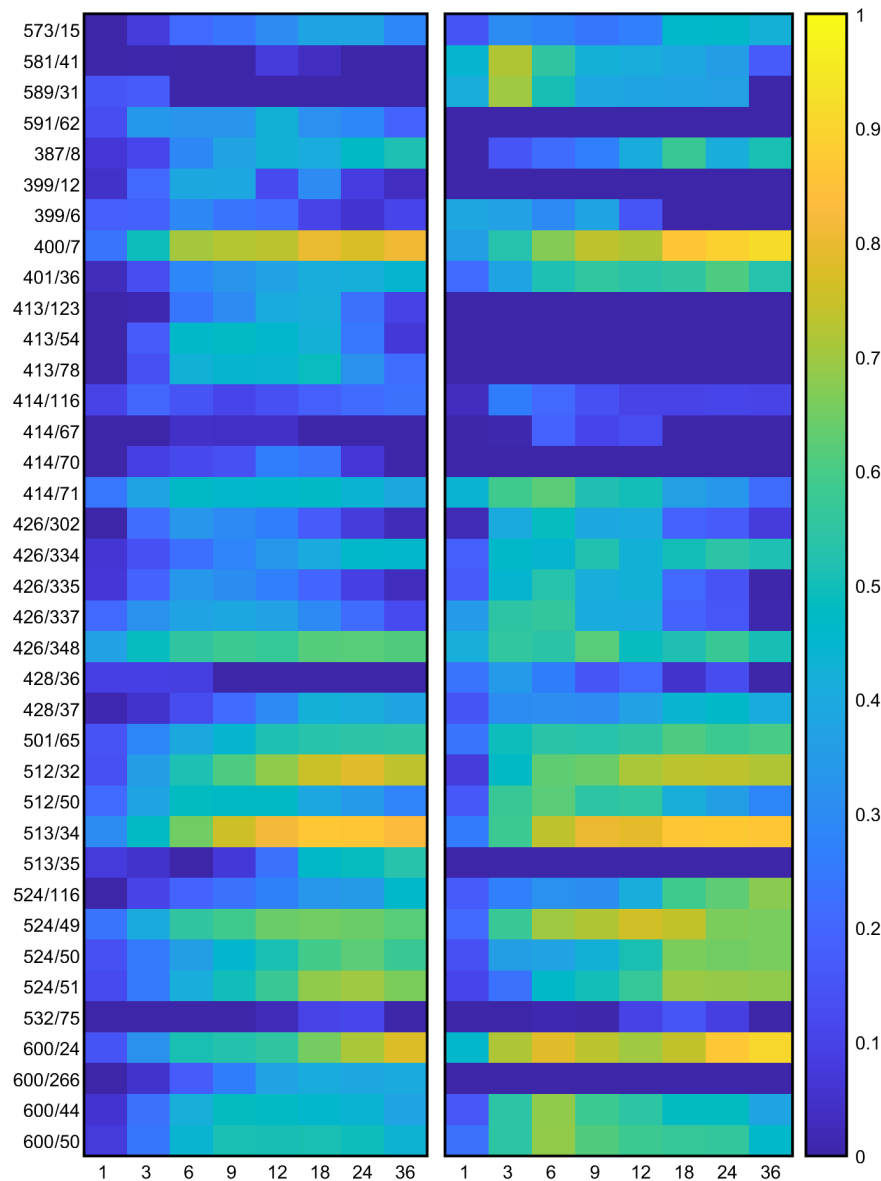


Figure 51. Portugal: Pearson correlation coefficients between groundwater levels observed at the 23 wells (y-axis) and the and SPEIs at the time scale of 1, 3, 6, 9, 12, 18, 24 and 36 months (x-axes) considering all months (left) and February-April months (right)

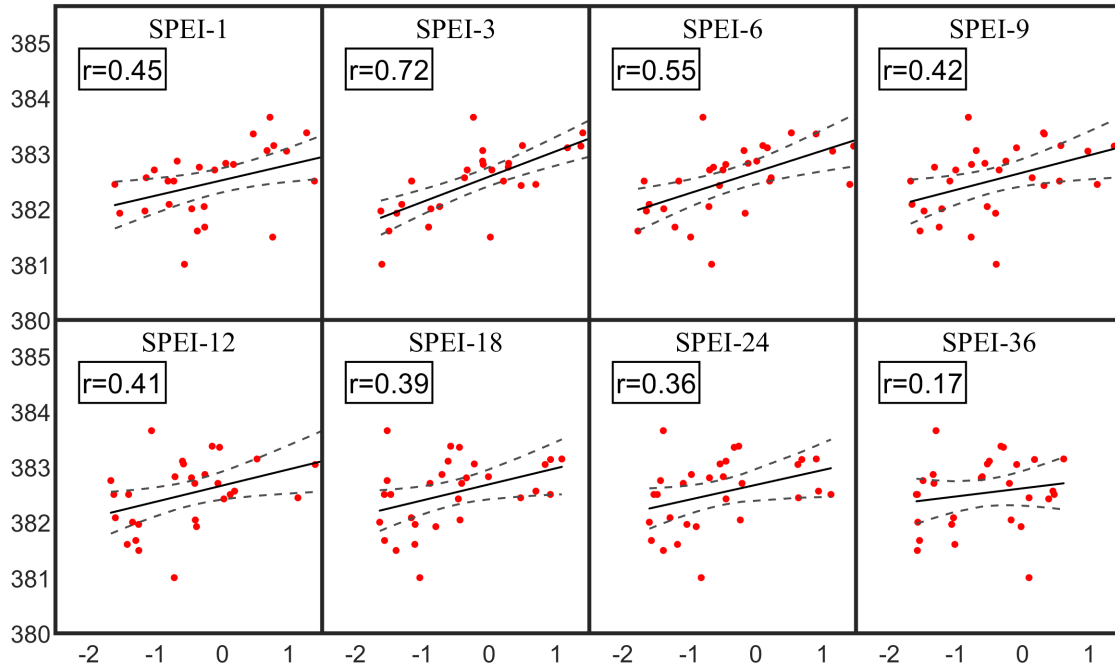


Figure 52. Portugal: linear regression model for the well 581/41. The x-axis shows the SPEI values and the y-axis the groundwater level in m a.s.l. The points are the observed groundwater levels, the solid line is the regression line and the dashed lines are the confidence intervals (95%); the correlation coefficients are reported in the boxes

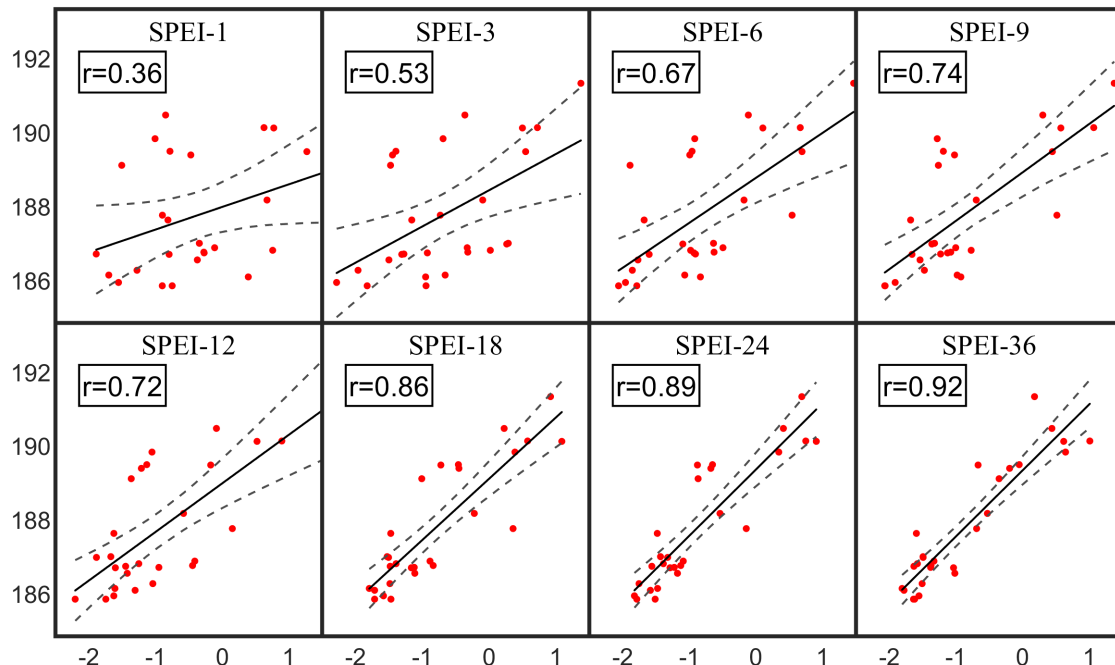


Figure 53. Portugal: linear regression model for the well 400/7. The x-axis shows the SPEI values and the y-axis the groundwater level in m a.s.l. The points are the observed groundwater levels, the solid line is the regression line and the dashed lines are the confidence intervals (95%); the correlation coefficients are reported in the boxes



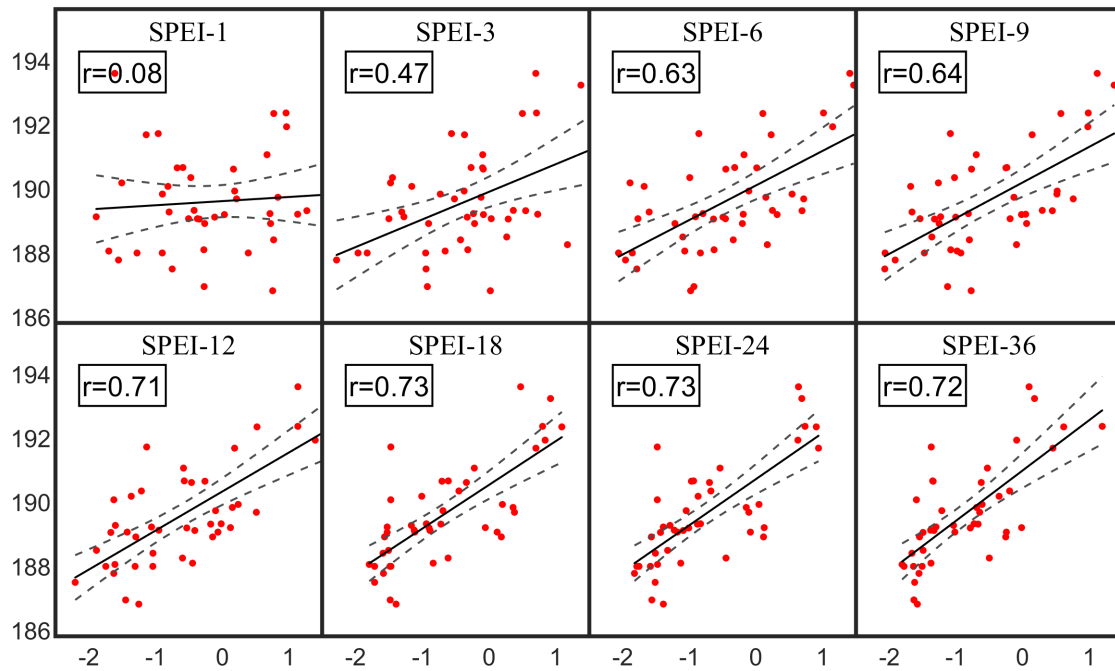


Figure 54. Portugal: linear regression model for the well 512/32. The x-axis shows the SPEI values and the y-axis the groundwater level in m a.s.l. The points are the observed groundwater levels, the solid line is the regression line and the dashed lines are the confidence intervals (95%); the correlation coefficients are reported in the boxes

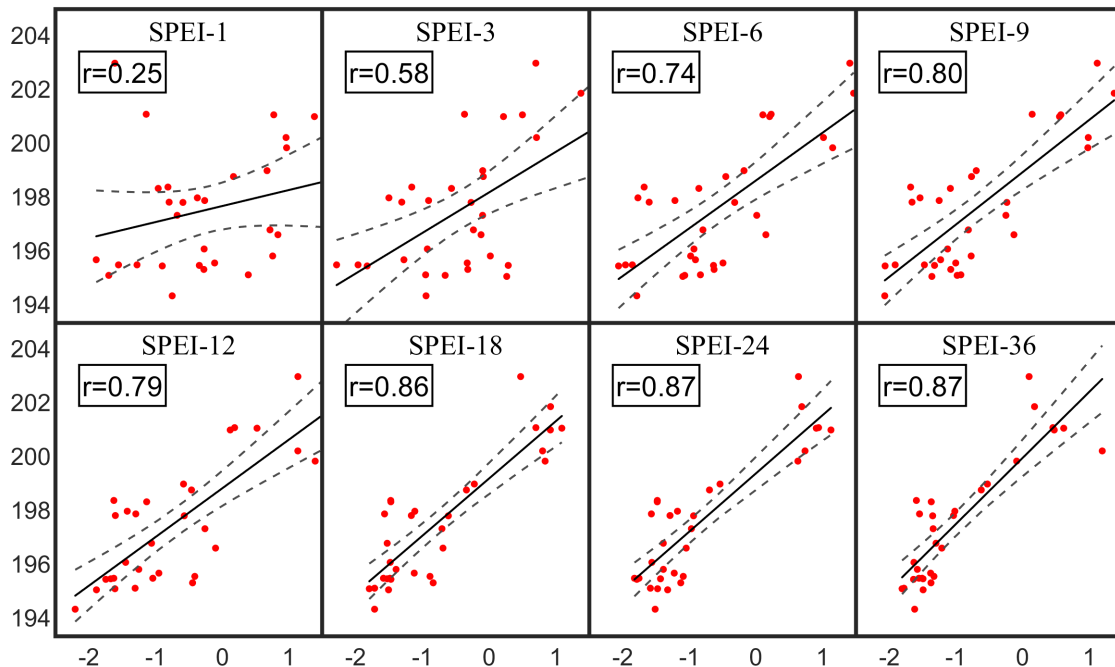


Figure 55. Portugal: linear regression model for the well 513/34. The x-axis shows the SPEI values and the y-axis the groundwater level in m a.s.l. The points are the observed groundwater levels, the solid line is the regression line and the dashed lines are the confidence intervals (95%); the correlation coefficients are reported in the boxes

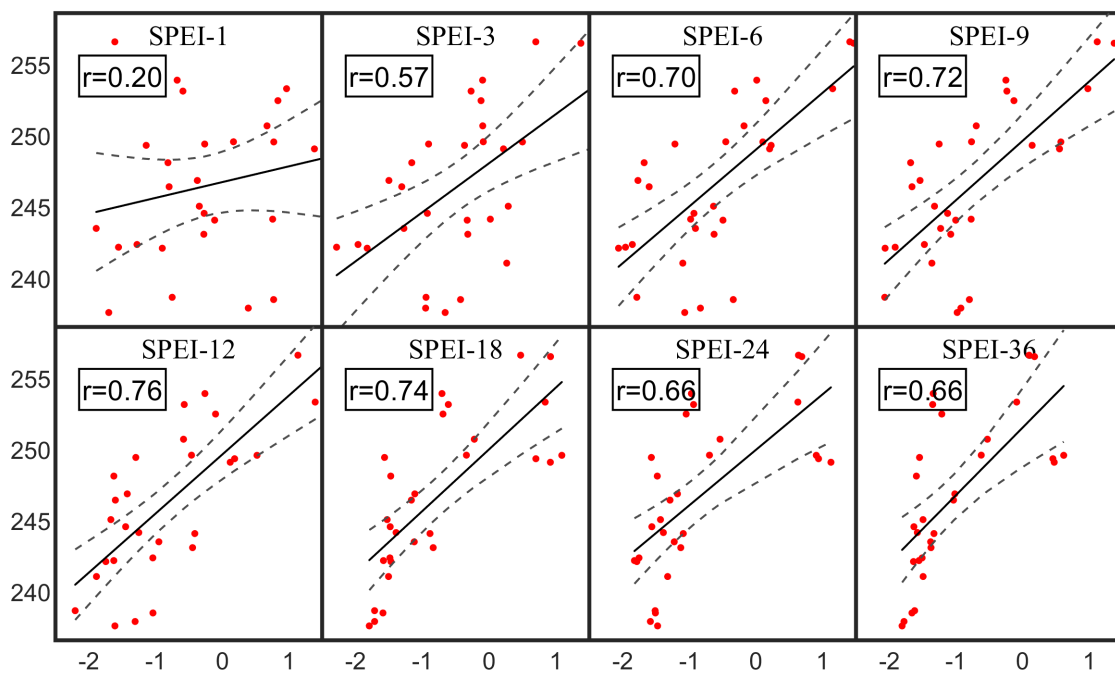


Figure 56. Portugal: linear regression model for the well 524/49. The x-axis shows the SPEI values and the y-axis the groundwater level in m a.s.l. The points are the observed groundwater levels, the solid line is the regression line and the dashed lines are the confidence intervals (95%); the correlation coefficients are reported in the boxes

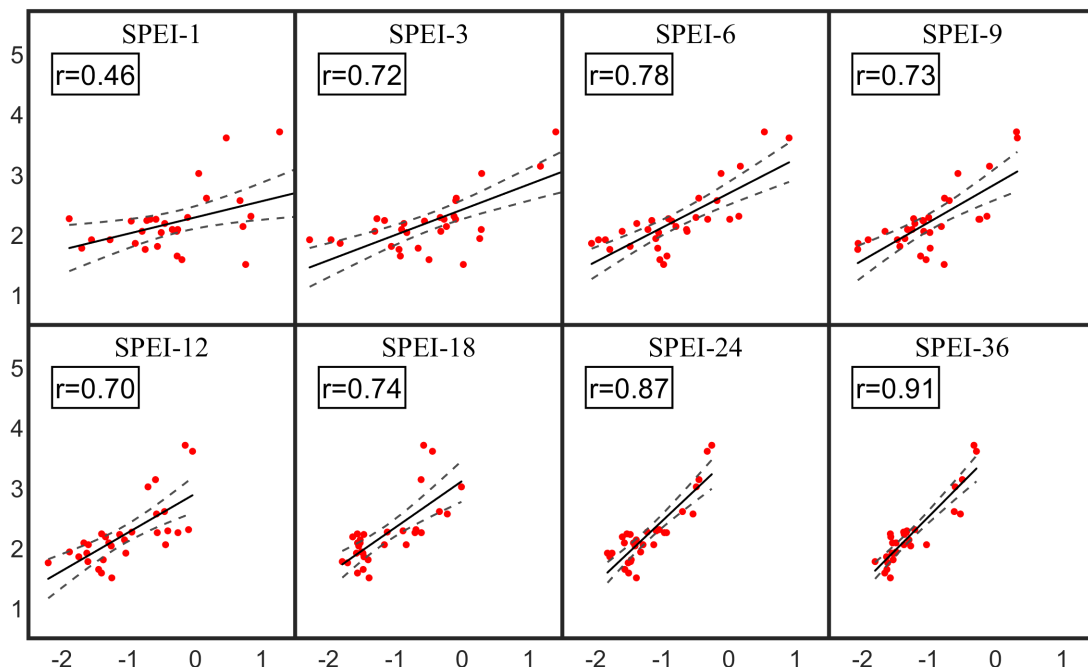


Figure 57. Portugal: linear regression model for the well 600/24. The x-axis shows the SPEI values and the y-axis the groundwater level in m a.s.l. The points are the observed groundwater levels, the solid line is the regression line and the dashed lines are the confidence intervals (95%); the correlation coefficients are reported in the boxes

### 3. References

- Allen, R.G., Pereira, L.S., Raes, D., Smith, M., 1998. FAO Irrigation and Drainage Paper No. 56 - Crop Evapotranspiration.
- Bakker, M., Post, V., Langevin, C. D., Hughes, J. D., White, J. T., Starn, J. J. and Fienen, M. N. (2016). Scripting MODFLOW Model Development Using Python and FloPy: *Groundwater*, v. 54, p. 733–739, doi:10.1111/gwat.12413.
- Biau, G. (2012). Analysis of a random forests model. *The Journal of Machine Learning Research*, 13(1), 1063-1095.
- Breiman, L. (2001). Random forests. *Machine learning*, 45(1), 5-32.
- Chen, T., & Guestrin, C. (2016, August). Xgboost: A scalable tree boosting system. In *Proceedings of the 22nd acm sigkdd international conference on knowledge discovery and data mining* (pp. 785-794), <https://doi.org/10.1145/2939672.2939785>.
- Cutler, A., Cutler, D. R., & Stevens, J. R. (2012). Random forests. In *Ensemble machine learning* (pp. 157-175). Springer, Boston, MA.
- Freund, Y., & Schapire, R. E. (1997). A decision-theoretic generalization of on-line learning and an application to boosting. *Journal of computer and system sciences*, 55(1), 119-139.
- Haitjema, H.M., Mitchell-Bruker, S., 2005. Are water tables a subdued replica of the topography? *Ground Water* 43(6), 781-786. DOI:10.1111/j.1745-6584.2005.00090.x.
- Harbaugh, A.W. (2005). MODFLOW-2005, the U.S. Geological Survey modular ground-water model -- the Ground-Water Flow Process: U.S. Geological Survey Techniques and Methods 6-A16.
- Pérez-Martín, Miguel A. (2005). Modelo Distribuido de Simulación del Ciclo Hidrológico y Calidad del Agua, Integrado en Sistemas de Información Geográfica, para Grandes Cuencas. Aportación al Análisis de Presiones e Impactos de la Directiva Marco del Agua. Universidad Politècnica de València.

- Python Core Team (2015). Python: A dynamic, open source programming language. Python Software Foundation. URL <https://www.python.org/>.
- Secci, D., Tanda, M. G., D'Oria, M., Todaro, V., & Fagandini, C. (2021). Impacts of climate change on groundwater droughts by means of standardized indices and regional climate models. *Journal of Hydrology*, 603, 127154.
- Seo, H. S., Šimůnek, J., Poeter, E. P. (2007). Documentation of the HYDRUS Package for MODFLOW-2000, the U.S. Geological Survey Modular Ground-Water Model, GWMI 2007-01, Int. Ground Water Modeling Center, Colorado School of Mines, Golden, CO, 96 p., 2007.
- Šimůnek, J., van Genuchten, M. Th., Šejna, M. (2005). The Hydrus-1D software package for simulating the one-dimensional movement of water, heat, and multiple solutes in variably-saturated media, Version 3.0, HYDRUS Software Series 1, Department of Environmental Sciences, University of California Riverside, Riverside, CA, 270 pp.
- TAGEM (2017). Türkiye'de Sulanan Bitkilerin Bitki Su Tüketimleri (Water Demand of The Crops Irrigated in Turkey). Ankara.
- TUIK (Turkish Statistical Institute) (2020). Database for agricultural area, crop pattern, biomass, and livestock; [www.tuik.gov.tr](http://www.tuik.gov.tr)
- Varouchakis, E.A., 2017. Spatiotemporal geostatistical modelling of groundwater level variations at basin scale: a case study at Crete's Mires Basin. *Hydrology Research*, 10.2166/nh.2017.146. DOI:10.2166/nh.2017.146.
- Varouchakis, E.A., Hristopulos, D.T., 2019. Comparison of spatiotemporal variogram functions based on a sparse dataset of groundwater level variations. *Spatial Statistics* 34, 100245. DOI:<https://doi.org/10.1016/j.spasta.2017.07.003>.
- Vicente-Serrano, S. M., Beguería, S. & López-Moreno, J. I. (2010). A multiscalar drought index sensitive to global warming: The standardized precipitation evapotranspiration index. *Journal of Climate* 23(7), 1696–1718.

Weedon, G.P., Gomes, S., Viterbo, P., Osterle, H., Adam, J.C., Bellouin, N., Boucher, O., and Best, M. 2010. WATCH Technical Report No. 22 - THE WATCH FORCING DATA 1958-2001: A METEOROLOGICAL FORCING DATASET FOR LAND SURFACE- AND HYDROLOGICAL-MODELS.

Yilmaz, G., Çolak, M. A., Özgencil, I., B., Korkmaz Metin, M., Korkmaz, M., Ertuğrul, S., Soyluer, M., Bucak, T., Tavşanoğlu, U. N., Özkan, K., Akyürek, Z., Beklioğlu, M., & Jeppesen E., (2021). Decadal changes in size, salinity, waterbirds, and fish in lakes of the Konya Closed Basin, Turkey, associated with climate change and increasing water abstraction for agriculture, *Inland Waters*, DOI: 10.1080/20442041.2021.1924034.